Journal of Catalysis 269 (2010) 201–218

Contents lists available at ScienceDirect

Journal of Catalysis

journal homepage: www.elsevier.com/locate/jcat

Formation of acid sites in amorphous silica-alumina

E.J.M. Hensen *, D.G. Poduval, P.C.M.M. Magusin, A.E. Coumans, J.A.R. van Veen

Schuit Institute of Catalysis, Eindhoven University of Technology, P.O. Box 513, 5600 MB Eindhoven, The Netherlands

ARTICLE INFO

Article history:
Received 26 August 2009
Revised 5 November 2009
Accepted 8 November 2009
Available online 11 December 2009

Keywords:
Amorphous silica-alumina
Acidity
Preparation
Deposition-precipitation

ABSTRACT

A suite of amorphous silica-aluminas (ASAs) was prepared by homogeneous deposition–precipitation (HDP) of aluminium on a silica surface followed by calcination. The HDP process was investigated in detail by ^{27}Al NMR spectroscopy of solid and liquid aliquots of the synthesis mixture. Deposition occurs predominantly via a hydrolytic adsorption of aluminium onto the hydroxyl groups of the silica surface. Precipitation becomes more significant at higher aluminium concentration. Depending on the aluminium loading, the surface contains four- and six-coordinated aluminium as well as patches of aluminium hydroxides. Calcination results in two competing process, that is the diffusion of aluminium into the silica network and sintering of aluminium into separate patches of a phase which mainly consists of octahedral Al. These ASAs exhibit Brønsted acidity similar to industrial amorphous silica-aluminas prepared by the grafting of aluminium on very reactive silica gels. Their acidity does not vary systematically with the aluminium concentration, except below 5 wt% Al_2O_3. The acidity increases with the calcination temperature. The active sites form due to the diffusion of aluminium into the silica network at high temperatures, leading to Al substitutions of Si atoms. This is expected as the acidity does not correlate with anything else, *viz.*, the amount of four-coordinated aluminium nor the presence of segregated Al or five-coordinated aluminium at the interface of these domains and the mixed silica-alumina phase. The surface of an amorphous silica-alumina consists of isolated aluminium grafted onto the silica surface (pure silica-alumina phase) with a very small amount of aluminium in the silica network, which brings about the Brønsted acidity, and small patches of aluminium oxides.

1. Introduction

Amorphous silica-alumina (ASA) is widely used as a solid acid catalyst in various chemical reactions including hydrocracking, isomerization and alkylation, which are important in the oil refining and petrochemical industry [1,2]. Hydrocracking involves a boiling-point shift of heavier fractions of crude oil towards lighter product streams through sequential steps of dehydrogenation of paraffins, β-scission of intermediate olefins and hydrogenation of the smaller olefins to paraffins. The catalysts are bifunctional and contain most often mixed metal sulfides for (de)hydrogenation and a cracking component of variable Brønsted acidity. As, at least in Europe, the demand for middle distillates is strongly increasing, balanced acidity in these catalysts to achieve high conversion, yet with high selectivity to diesel and kerosene fractions, is pivotal. Here, ASAs with only moderate acidity are preferred. Besides, the present-day composite hydrocracking catalysts nearly always contain an ASA component next to steam-stabilized faujasite zeolite.

Accurate control of the acidic properties of ASAs is hampered by two factors: a lack of the understanding of the origin of Brønsted acidity in these mixed oxides and the inhomogeneous composition resulting from typical preparation methods. Regarding the former, the nature of the Brønsted acid sites (BAS) has not been unequivocally established. The more widely shared opinion is that the Brønsted acidity derives from tetrahedral Al^{3+} in the silica network, as initially proposed by Thomas [3] and Tamele [4] in the late 1940s. However, evidence in this debate remains inconclusive, because the corresponding strongly acidic bridging hydroxyl groups, which should be similar in nature to those well-established in crystalline zeolites, have eluded direct spectroscopic observation until now. Thus, alternative explanations for ASA's acidity have been invoked. These include Lewis acidic Al ions substituting for the protons of surface silanol groups [5,6] and the higher acidity of silanol groups in the presence of neighbouring aluminium surface atoms [7]. The latter model forms the basis for the more recent proposals of paired (SiOH and Al) sites [8–10], which involve aluminium as part of the silica network or of an interface region between silica and alumina [11,12]. The interface in the latter interpretation is made up by five-coordinated Al. Similarly, controversy exists about the intrinsic acidity of the protons in ASAs, which is thought to differ from that in zeolites. The higher flexibility of the bonds around the bridging hydroxyl groups in a non-crystalline material may explain the lower acidity [13]. A crucial question is whether the

* Corresponding author.
E-mail address: e.j.m.hensen@tue.nl (E.J.M. Hensen).

0021-9517/$ - see front matter © 2009 Elsevier Inc. All rights reserved.
doi:10.1016/j.jcat.2009.11.008

overall Brønsted acidity in ASAs is caused by a few strongly acidic sites or by a large number of weaker ones.

The other reason that surface acidity of ASAs is understood to a much lesser extent than that of zeolites relates to the complex surface composition of these mixed oxides. ASAs are made by co-precipitation, cogelation or grafting processes [14–16], and the content of alumina is between 5 and 60 wt%. In nearly all cases, the resulting materials contain a non-random distribution of aluminium in silica, because the formation of Al–O–Al bonds is faster than that of Al–O–Si bonds [17–19]. Besides isolated aluminium ions on the silica surface, small clustered aluminium oxides are present ranging from nanoclusters up to sizes where rather the presence of a separate alumina-type phase should be considered [20]. Obviously, depending on the preparation route and further calcination aluminium can end up in the silica network as a substituent for tetrahedral Si [20–22]. The negative charge of the silica following the substitutions of Si for Al can be compensated by protons at the surface which could in principle display strong Brønsted acidity, or by internal silanol groups [23] and surface mono- or polymeric hydroxyaluminium cations [20].

The present project was undertaken with the aim of (i) synthesizing a set of ASA materials by as controlled a method as possible for future use in catalytic studies and (ii) learning more about the genesis of Brønsted acid sites in ASAs and their strength. The synthesis method chosen was a well-defined variant of grafting, *viz.*, homogeneous deposition–precipitation [24]. An acidic starting solution of Al^{3+} is homogeneously basified through thermal decomposition of urea in the presence of a silica aerogel. Urea slowly decomposes in aqueous solutions when the temperature is raised above 343 K, which ensures a slow homogeneous release of hydroxyl anions and avoids pH inhomogeneities as would be present when a base is added dropwise. As urea decomposition proceeds rather slowly, the hydrolysis of Al can be followed by ^{27}Al NMR spectroscopy [25]. Thus, one can in principle follow the deposition of aluminium on silica as a function of pH and the initial aluminium concentration. The precursors are subsequently calcined to give the desired ASAs. These materials are compared to ASAs prepared by cogelation [15], alumination of silica by $(NH_4)_3AlF_6$ [26] and the co-condensation of an organometallic double alkoxide containing silicon and aluminium with tetramethoxysilane [27]. ^{27}Al NMR spectroscopy will be the main technique to follow the aluminium coordination during its deposition on silica and upon further calcination. The acidity of the calcined support materials is evaluated from their acid catalytic activity in the hydroconversion of *n*-heptane, after loading with palladium, under conditions where the isomerization step is rate limiting, and compared to that of a commercial ASA.

As an introduction, the various structures to which the presence of six-, five- and four-coordinated Al atoms in amorphous silica-aluminas has been assigned are described here in some detail. This discussion is guided by Table 1, which summarizes the most important structural models of aluminium-containing phases in ASAs. The early work of De Boer [5] discussed the binding of Al to two or three vicinal silanol groups on the surface and the resulting surface tetrahedral Al ion was coined to be the acidic site. Tamele [4] suggested the reaction of $Al(OH)_3$ with three silanol groups. The substitution of Si by Al with the respective formal charges of 4+ and 3+ in the silica network [3,4] induces a negative charge on the oxygen atoms around the Al atoms, which is compensated by cations. This view was further developed by Fripiat and coworkers [20–22] and Boehm and Schneider [28]. Boehm and Schneider mention that high temperature calcination facilitates the diffusion of aluminium into the silica network. The model of Fripiat describes ASAs in terms of a negatively charged aluminosilicate core and positively charged surface species. When the negative charge is formed by a surface substitution of Si by Al and is compensated by a proton, a truly BAS should be obtained. Tetrahedral Al can also become a part of a transitional alumina phase which may form following segregation during the preparation and upon calcination. Likewise, the presence of octahedral coordination of Al in these amorphous mixed oxides points to the presence of transitional aluminas or at least to some polymeric form of Al. Octahedral Al is the dominant coordination in many transitional aluminas [29,30]. Various authors [31,32] have also proposed that hydroxyaluminium cations present on the surface act as charge compensating cations.

The assignment of five-coordinated Al species in ASAs is under debate [33,34]. This coordination state has been identified in ^{27}Al NMR spectra as a resonance between 30 and 35 ppm for zeolites, phyllosilicates and ASAs [33,35,36]. For zeolites, such a species has been interpreted in terms of a distorted tetrahedral species [26], or as a part of an extraframework silica-alumina phase as typically found in steam-calcined zeolites [37]. In phyllosilicates, five-coordinated aluminium exists as an interface species between alumina and a mixed silica-alumina phase [36]. Similarly, five-coordinated aluminium in ASAs was assigned to the interface between an alumina-type phase and a truly mixed silica-alumina phase [31]. Five-coordinated Al has been identified as an intermediate coordination state during the strong atomic rearrangements during dehydration processes of alumina precursors [38–42].

More detailed information on the Al speciation is obtained by recording ^{27}Al NMR spectra before and after exposure to ammonia. The changes in the Al coordination upon exposure to ammonia for aluminosilicates have been described by several groups [43,44]. For BETA [43] and faujasite zeolites [44], dehydration and adsorption of ammonia resulted in strong changes in the aluminium coordination: part of six-coordinated Al converted to a tetrahedrally coordinated species. The initial explanation has been that some framework octahedral Al^{3+} exhibit sixfold coordination with four framework oxygen species, an hydroxyl group and one water molecule [44]. A more reasonable explanation was put forward by Omegna et al. [37], who state that the flexible coordination in steam-calcined faujasite is limited to the aluminium atoms which are part of an extraframework phase with an amorphous silica-

Table 1
Assignments of four- (tetrahedral), five- (penta-coordinated) and six- (octahedral) coordinated aluminium atoms (^{27}Al NMR chemical shifts indicated by δ) in ASA.

Coordination	Assignments	References
Four ($\delta \approx 54$ ppm)	Grafted aluminium	De Boer [5]
	Aluminium isomorphously substituting Si^{4+} in silica	Thomas [3], Tamele [4], Hansford [7], Boehm and Schneider [28]
	Four-fold coordinated aluminium in (transition) aluminas	MacKenzie et al. [29,30]
Five ($\delta \approx 30$–35 ppm)	Interface between alumina and silica or aluminosilicate	de Witte et al. [33]
	Five-fold coordinated aluminium in transition aluminas	MacKenzie et al. [29,30]
	Distorted tetrahedral species	Peeters and Kentgens [34]
	Associated with ASA phase	Williams et al. [31], Omegna et al. [37]
Six ($\delta \approx 0$ ppm)	γ-Al_2O_3 after calcination	*e.g.* MacKenzie et al. [29,30]
	Amorphous polymeric aluminium oxide (boehmite) phase	Cloos et al. [20]
	Charge-compensating cation	Williams et al. [31], Stone et al. [32]

alumina character. Similarly, in ASAs only those aluminium atoms associated with a mixed phase change their coordination upon ammonia adsorption. The aluminium atoms that are a constituent of a separate alumina-type phase do not change their coordination [31].

2. Experimental section

2.1. Synthesis of materials

2.1.1. Homogeneous aluminium deposition–precipitation

ASAs were prepared by the deposition of aluminium on silica by a homogeneous basification of an aqueous starting solution containing aluminium nitrate. The starting materials were a commercial silica (Sipernat-50, Degussa, surface area 400 m^2/g, hydroxyl density 4.1 OH/nm^2), $Al(NO_3)_3{\cdot}9H_2O$ (Merck, purity 99%) and urea (Merck, purity 99%). The hydroxyl density of silica was determined from the weight loss between 473 and 1073 K in a TGA experiment. In a typical synthesis, silica was suspended in demineralized water together with the desired amount of aluminium nitrate and urea in a stirred double-walled reaction vessel. The initial aluminium concentration ($[Al]_0$) was varied between 0.03 and 0.11 M, while the urea concentration was kept constant at 0.76 M. To prepare an ASA with a higher alumina content, a synthesis was carried out at $[Al]_0$ = 0.16 M and a urea concentration of 1.1 M. The temperature of the well-stirred suspension was increased to 363 K by circulating thermostat-controlled water between the inner and outer walls of the vessel. During the entire synthesis the pH of the suspension was monitored. The aluminosilicates were recovered by filtration, washed with demineralized water and dried at 393 K and finally calcined in static air at 773 K or 1073 K. The samples are denoted by ASA(*X*/*Y*, *T*), where *X* and *Y* refer to the alumina and silica contents by weight and *T* refers to the calcination temperature. Unless stated otherwise, the loadings of Al are expressed as a weight percentage of Al_2O_3. In a set of related syntheses, the suspension was removed from the reaction vessel at a certain pH and cooled in an ice-bath to prevent further decomposition of urea. The resulting materials are denoted by ASA(*X*/*Y*, *S*, *T*) where *S* stands for the pH at which the synthesis mixture was unloaded. To compare the influence of the silica source, fumed silica (VWR, surface area 390 m^2/g, hydroxyl density 1.2 OH/nm^2 from TGA) was used to prepare ASA(5/95,fumed).

2.1.2. Cogelation

Sodium silicate (Merck, 30 wt% SiO_2) was added under vigorous stirring to a solution of aluminium chloride (Merck, 99%), following a modification of a patent recipe [15]. The pH was brought to seven with acetic acid and the mixture was further stirred for 1 h. The sample was then recovered by filtration and washed repeatedly with distilled water. Ion-exchange with 0.3 M NH_4NO_3 solution was carried out seven times under refluxing to remove the sodium ions. The final sodium content was below 0.1 wt%. The material was finally dried overnight at 393 K and calcined in static air at 923 K for 4 h. This sample is referred to as ASA(5/95,cogel).

2.1.3. Alumination of SiO_2

Alumination of a silica was carried out with ammonium aluminiumhexafluoride [26]. First, ammonium hydroxide was added to an aqueous suspension of silica (Sipernat-50) to adjust the pH to 9. An aqueous solution of $(NH_4)AlF_6$ (Alfa-Aesar, 99%) was then added slowly in 1 h to obtain the desired amount of aluminium (SiO_2/Al_2O_3 = 19). The resulting solution was stirred overnight at room temperature. The sample was recovered by filtration, washed with distilled water and dried overnight at 393 K. The sample was then calcined at 773 K for 4 h and is referred to as ASA(5/95,F).

2.1.4. Organometallic precursor

An organometallic route consisted of mixing tetramethylorthosilicate (TMOS, Merck, 99%) with an amount of di-*sec*-butoxyaluminotriethoxysilane (Alfa Aesar) to obtain a homogeneous mixture. The ratio of TMOS and the double alkoxide was chosen such that a final SiO_2/Al_2O_3 ratio of 4 was obtained. To this mixture, 40 ml of water was added and stirred overnight at room temperature. The solution was then transferred into an autoclave and kept at 373 K for 72 h. The sample was recovered by filtration, washed with water, dried overnight at 393 K and finally calcined at 823 K for 4 h. This sample is designated ASA(20/80,alkoxide).

2.1.5. Commercial samples

A commercial ASA reference sample (55 wt% Al_2O_3) prepared by grafting aluminium to *in situ* prepared silica gel at pH 3 was used as received. The ASA was calcined at 773 K and 1073 K. These samples are denoted by ASA(comm). An ultrastabilized Y zeolite with a silica-to-alumina ratio of 9.3, denoted by USY(9.3), was used as received from Zeolyst International.

2.2. Characterization

The elemental composition of the calcined ASAs was determined by ICP analysis. Prior to analysis on a Spectro CIROS^{CCD} ICP optical emission spectrometer, the samples were dissolved in a mixture of stoichiometric ratio by volume of hydrofluoric acid, nitric acid and water.

Thermogravimetric analysis was carried out for the parent silicas on a Shimadzu TGA-50 equipped with a platinum sample holder. The samples were heated in air at a rate of 10 K/min to 1073 K. The hydroxyl density of the silica supports was calculated from the water loss between 473 K and 1073 K.

The surface area of the ASAs was determined from N_2 adsorption measurements at liquid nitrogen temperature with a Micromeritics Tristar 3000. Prior to the measurements, the samples were dried at 573 K for 3 h. The surface areas were determined using the Brauner–Emme– Teller method.

Magic-angle spinning (MAS) ^{27}Al NMR spectra were recorded on a Bruker DMX500 spectrometer operating at an Al NMR frequency of 130 MHz and equipped with a 4-mm MAS probe head. The ^{27}Al chemical shifts are referenced to a saturated $Al(NO_3)_3$ solution. An accurately weighed amount of sample was packed in a 2.5 mm zirconia rotor. Typically, the aluminosilicates were exposed to a saturated water vapour at room temperature overnight. The sample rotation speed was 25 kHz. For quantitative MAS ^{27}Al NMR spectra single-pulse excitation was used with a single 36° pulse of 2 μs and an interscan delay of 1 s. It was checked for a few typical samples that shortening the excitation pulse to 1 μs or increasing the interscan delay to 2 or 5 s did not affect the relative signal intensities in the spectra.

^{27}Al MQMAS NMR spectra with a zero-quantum filter were recorded by the use of the three-pulse sequence p_1-t_1-p_2-τ-p_3-t_2 with strong pulses p_1 = 3.0 μs, p_2 = 1.2 μs at a radio-frequency field strength of 150 kHz and a weak pulse p_3 = 11 μs at a field strength of 7 kHz. The evolution time t_1 was sampled with 64 time increments of 20 μs, the signal was recorded during t_2 with a sample time of 10 μs up to 10.3 ms and the filter time τ was 20 μs. Another set of NMR experiments was carried out for amorphous silica-aluminas after dehydration and adsorption of ammonia. To this end, an amount of sample was heated in a flow of He from room temperature to 393 K at a rate of 6 K/min followed by exposure to a flow of 1 vol.% NH_3 for 1 h. The sample was then cooled to room temperature in the same gas mixture and was transferred into a nitrogen-flushed glovebox to be packed into a 2.5 mm NMR rotor.

Rotational-resonance ^{27}Al NMR experiments were carried out by using the pulse sequence $\theta_{+x} - \tau - \theta_{\pm x} - t_{mix} - \theta\phi - t_2$ with $\theta \sim 30°$ pulses of 1.8 μs. The sample-rotation rate ν_r was matched to the frequency separation $\Delta\nu$ between the tetrahedral and octahedral Al signals at, respectively, ~56 and ~6 ppm, $\nu_r = \Delta\nu \sim 6.5$ kHz. The interval τ was adjusted to ½ $\Delta\nu$ of about 71 μs (corrected for the θ pulse duration). The carrier frequency was set $\Delta\nu$ upfield of the octahedral signal. Under these conditions, the $\theta_{+x} - \tau - \theta_{\pm x}$ sequence produces tetrahedral and octahedral Al polarization with opposite signs. The polarization of either the octahedral or the tetrahedral ^{27}Al spin was inverted in an alternating way by changing the phase of the second pulse. After the selective inversion, the octahedral and tetrahedral Al spins were given the opportunity to exchange spin polarization during the following mixing time t_{mix}. The third θ pulse at the end of t_{mix} rotates the respective polarization vectors of the octahedral and tetrahedral sites into the xy plane, and the corresponding NMR signals are measured during the acquisition time t_2 with a scan accumulation scheme following the alternating sign of the second pulse and the phase ϕ of the third pulse. For comparing the polarization exchange to the recovery of the polarization caused by spin-lattice relaxation, also a background experiment with equal polarization perturbation of the octahedral and tetrahedral Al sites was carried out by taking $\tau = 2.5$ μs. A phenomenological bi-exponential decay

$$R(t) = A \cdot \exp(-t/T_{1A}) + B \cdot \exp(-t/T_{1B}) \quad (1)$$

is fitted to the background decay. With $R(t)$ determined from the background decay, the rotational-resonance exchange data are then fitted with a model of the form

$$I(t) = I(0)A_T \cdot \exp(-t/\tau_{se}) + 1 - A_T \cdot R(t) \quad (2)$$

MAS ^{29}Si NMR spectra were recorded on a Bruker DMX500 operating at Si NMR frequency of 99 MHz. Direct ^{29}Si excitation with a single 90° pulse of 5 μs was combined with high-power proton decoupling and a recycle delay of 180 s between subsequent scans. Tetramethylsilane (TMS) was used as an external reference for the chemical shift.

Electron microscopy analysis was done using a JEOL 2100F transmission electron microscope (TEM) interfaced with a ThemoNoran NSS energy dispersive X-ray spectrometer. The TEM was operated at 200 kV. Sections of the sample were prepared by embedding the powder in polymethylmethacrylate and using an ultramicrotome (model Leica EM UC6) to prepare sections with a nominal thickness of 50 nm. The local variation in the composition of the samples was measured using energy dispersive X-ray spectrometry (EDS). Two linescans were collected from each sample in the scanning mode with a nominal spot size of 1 nm. A typical measurement consisted of 100 equally spaced points along a line approximately 5 μm long. The dwell time per point was 100 and 30 s for ASAs with alumina contents of 5 and 20 wt%, respectively. The relative elemental concentration was calculated using the Cliff-Lorimer method without any absorption corrections. Peak fitting was made using a digital top hat filter to remove the background from the spectra before fitting the spectrum with a reference spectrum.

The concentration of strong Brønsted acid sites in the aluminosilicates was evaluated from catalytic activity measurements in the hydroconversion of n-heptane of Pd-loaded aluminosilicates. To this end, a sieve fraction (177–420 μm) of the dried support was loaded with 0.4 wt% Pd via incipient wetness impregnation with a solution of appropriate concentration of $Pd(NH_3)_4(NO_3)_2$. The resulting materials were calcined at 573 K. Prior to testing, the catalysts were reduced at 713 K at 30 bar in flowing hydrogen. Hydroconversion of n-heptane was carried out at 30 bar at a H_2/hydrocarbon ratio of 24 mol/mol. The reaction temperature was lowered from 713 K till 473 K at a rate of 0.2 K/min. The kinetics of bifunctional, aluminosilicate-catalyzed hydroconversion of n-alkanes is well understood [45,46]. n-Heptane hydroconversion involves the dehydrogenation of n-heptane by the noble metal phase, isomerization or β-scission by strong Brønsted acid sites and hydrogenation of the i-olefins to i-paraffins. Meeting the requirement of sufficient hydrogenation activity is easily met if the metal loading is not too low (see Supporting Information). In such case, the Brønsted acid-catalyzed conversion step of the intermediate olefins via carbenium-ion chemistry is rate limiting and the catalytic activity scales with the density of acid sites if their acidity is assumed to be constant. To verify this assumption, we have recently conducted an extensive spectroscopic study, involving H/D exchange with C_6D_6, which shows that it is only the relatively homogeneous group of strong acid sites of zeolitic strength that is responsible for the isomerization activity [47]. The activity of the catalyst is expressed as the temperature at which a hydrocarbon conversion of 40% was achieved. Assuming first-order kinetics in the reactant hydrocarbon and a constant pre-exponential factor, we can relate the number of acid sites (N'_{iso}) to the temperature required to obtain a conversion of n-heptane of 40% (T_{40}) according to

$$\ln N'_{iso} = C + \frac{E_{act}}{RT_{40}} \quad (3)$$

in which E_{act} (kJ mol^{-1}) is the activation energy, R (kJ mol^{-1} K^{-1}) is the gas constant and C is a constant. Hence, the term E_{act}/RT_{40} scales with the number of active sites.

3. Results and discussion

3.1. Homogeneous deposition–precipitation of aluminium on silica

The grafting of aluminium on silica as a function of $[Al]_0$ and the pH was investigated with the aim to prepare acidic ASA supports. In the acidic aqueous starting solution of $Al(NO_3)_3$ and urea, decomposition of urea via $(NH_2)_2CO + 3H_2O \rightarrow 2NH_4^+ + CO_{2g} + 2OH^-$ starts above 343 K [24], and results in a gradual and homogeneous release of hydroxyl anions in the well-stirred solution.

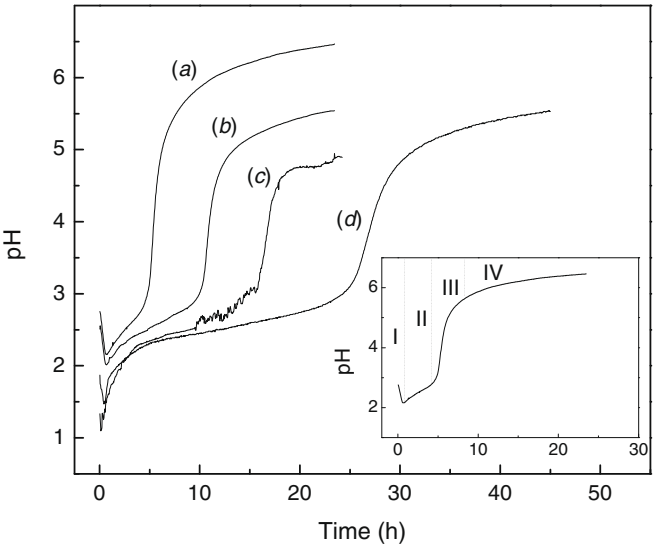

Fig. 1. Evolution of pH with time during homogeneous deposition–precipitation of aluminium on silica following the addition of aluminium nitrate to an aqueous suspension of silica aerogel containing urea. The temperature is then increased to 363 K. The initial aluminium concentration was varied to obtain ASAs with nominal alumina contents of 5 wt% (a), 10 wt% (b), 15 wt% (c) and 20 wt% (d). The inset indicates the various regions on the pH curve for ASA(5/95).

Fig. 1 shows the evolution of pH as a function of time and $[Al]_0$. Four main regions can be distinguished. Region I starts when the aluminium nitrate solution is added resulting in a decrease of the pH. At the same time the temperature of the solution is increased. The end point of Region I is defined as the minimum in the pH curve. This point corresponds to the state when the temperature of the solution exceeds 343 K, resulting in the start of urea hydrolysis. Initially, the pH increased quite strongly followed by a gradual increase of the pH. Region III is characterized by a steep increase of the pH and finally a relatively stable pH plateau defines region IV. The final pH of the synthesis mixture decreased with increasing $[Al]_0$ for ASAs with an alumina content up to 15 wt% as more OH^- was used to hydrolyze aluminium. The final pH of ASA(20/80) was higher than that of ASA(15/85) because of the higher urea concentration (1.1 M) employed to prepare ASA(20/80). An ASA(20/80) prepared at a urea concentration of 0.76 M had a final pH of 3.3 and the alumina content was only 16 wt%. Table 2 lists the composition and textural properties of the calcined ASAs. The surface areas and pore volumes decrease with increasing aluminium content.

Table 2
Textural properties of the various starting silicas and calcined ASAs. The final pH values and alumina contents of the ASA syntheses are given.

Sample	Final pH of synthesis	Al_2O_3 (wt%)	Surface area (m^2/g)	Pore volume (ml/g)[a]
Sipernat-50	–	–	400	n.d.
Fumed silica	–	–	390	n.d.
ASA(5/95)	6.2	5.1	410	2
ASA(10/90)	5.5	10.1	398	1.8
ASA(15/85)	4.3	15.1	380	1.6
ASA(20/80)	3.3	16	n.d.[c]	n.d.
ASA(20/80)[b]	5.5	20	354	1.4
ASA(5/95,3)	3	4.3	419	2
ASA(5/95,4)	4	5.1	412	2
ASA(10/90,3)	3	9	397	1.8
ASA(15/85,3)	3	12.1	373	1.6
ASA(20/80,3)	3	10	364	1.4
ASA(5/95,fumed)	6.5	4.2	400	2
ASA(5/95,cogel)	7	5	463	1.6
ASA(5/95,F)	9	5.1	402	2.1
ASA(20/80,DA)	–	20	372	1.4

[a] Water pore volume.
[b] Preparation at a urea concentration of 1.1 M.
[c] Not determined.

The deposition process of aluminium was studied in more detail by MAS ^{27}Al NMR spectroscopy. Firstly, the coordination of the Al species in the synthesis mixture and deposited on silica in ASA(5/95) was determined. Secondly, NMR spectra of ASA(5/95) at various stages of the synthesis were compared. In order to understand the deposition process, the Al^{3+} species in an aqueous solution as a function of pH was also studied. Similar to the work of Vogels et al. [25], the forced hydrolysis of Al was carried out in the presence of urea. For this experiment, the concentrations of aluminium nitrate and urea were 0.03 M and 0.7 M, respectively. Liquid samples were withdrawn from the solution and immediately cooled in an icebath to prevent further urea decomposition. Fig. 2 shows ^{27}Al NMR spectra of the liquid samples at pH 3, 4.7 and 5.5. At pH 3, the spectrum is dominated by a resonance at −0.11 ppm due to $Al(H_2O)_6^{3+}$. The resonance at −2.67 ppm is due to the replacement of one water ligand by urea in $[Al(H_2O)_5(urea)]^{3+}$ [48]. The broad peak around 4.4 ppm indicates the presence of dimeric $[Al_2(OH)_2(H_2O)_8]^{4+}$, or trimeric $[Al_3O_2(OH)_4(H_2O)_8]^{+}$ Al complexes [49,50]. At pH 4.7, the spectrum contains two resonances at 0.3 ppm and 63.0 ppm. Further hydrolysis of aquated Al^{3+} ions resulted in a downfield shift of the Al resonance and an

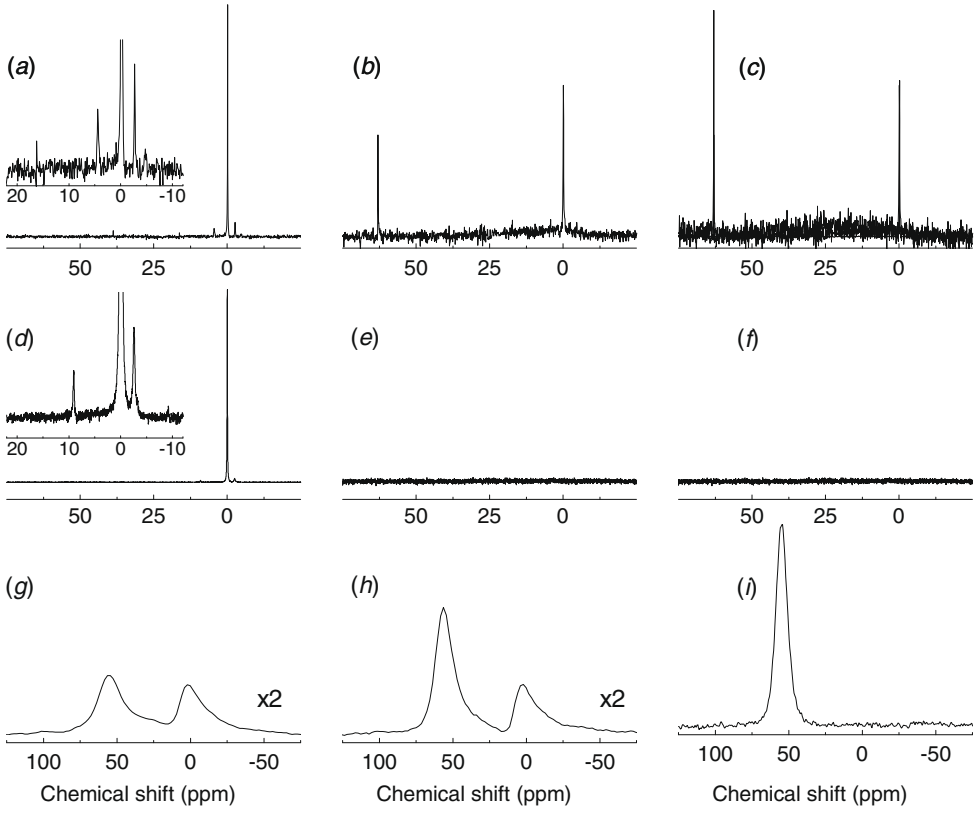

Fig. 2. ^{27}Al NMR spectra of an aqueous 0.03 M aluminium nitrate solution during urea (0.76 M) decomposition at a temperature of 363 K at pH 3 (a), pH 4.7 (b) and pH 5.5 (c). Spectra of the solution (d–f) and dried solids (g–i) removed during the preparation of ASA(5/95) at pH 3 (d, g), pH 4 (e, h) and pH 6.5 (f, i).

increase in the line width [51]. In line with the literature [25], the disappearance of the poly-aluminium complexes characterized by a resonance at 4.4 ppm goes with the appearance of a sharp signal around 63.0 ppm. This feature is caused by the symmetric tetrahedral coordination of Al in the Al_{13} complex $[AlO_4Al_{12}(OH)_{24}(H_2O)_{12}]^{7+}$ with the Keggin structure [52,53]. The octahedral Al in this complex, which has been reported to give a characteristic resonance around 12 ppm [25], is absent in our spectrum, probably as a result of the strong quadrupolar line broadening caused by the asymmetry around the Al nuclei. Therefore, the resonance around 0 ppm should be mainly due to hydrolyzed aluminium complexes. The spectrum at pH 5.5 contains a single resonance at 63.0 ppm, which indicates that the solution contains predominantly Al_{13} complexes. Under these conditions, neither a signal of $Al(OH)_4^-$ at 80 ppm [54] nor that of a suspected dimer Al_{13} complex at 70 ppm [55] is observed. As the pH rises above 5, the solution, which was clear at the beginning, becomes turbid which points to the onset of precipitation. Later, a distinct white precipitate is observed, which is pseudo-boehmite.

Subsequently, the synthesis of ASA(5/95) was examined by taking aliquots of the suspension at three stages: (i) at the end of region II (pH 3), (ii) during the strong pH increase in region III (pH 4) and (iii) at the end of region IV (pH 6.5). After cooling, the solid was immediately separated from the liquid by a filter (Millipore, 0.4 μm) and ^{27}Al NMR spectra of the liquid and the dried solid were recorded. The resulting spectra and the loadings of the solids are given in Fig. 2 and Table 2, respectively. In region II, the coordination number of Al in the solution is 6 as follows from the dominance of the signals at −0.11 and −2.67 ppm. The signal at 4.4 ppm is absent and instead a weak resonance around 9 ppm is observed. The assignment of this signal is not clear, but various six-fold coordinated species have been observed between 12.6 and 4 ppm [25]. The Al content of the solid extracted at pH 3 is 4.3 wt% Al_2O_3. Thus, a large part of the Al has been grafted already to the surface at relatively low pH. A substantial part (60%) is present in tetrahedral coordination (Al^{IV}, ∼55 ppm) on the silica surface, the remaining Al species are in octahedral coordination (Al^{VI}, ∼1.8 ppm). In the middle of region III at pH 4, all Al has been grafted onto the silica surface, as the solid contains the 5.1 wt% Al_2O_3. In line with this, no Al is detected in the solution extracted at pH 4. Compared to the sample at pH 3, the solid contains a higher contribution of Al^{IV} (70%). After completion of the synthesis, the solid contains exclusively Al^{IV} species. As the final ASA(5/95) and the sample extracted at pH 4 contain the same amount of Al, it follows that the atomic organization around the grafted Al^{3+} has changed markedly in region III.

In a similar manner, ^{27}Al NMR spectra of the ASAs with a higher alumina content extracted at pH 3 and after the completion of the synthesis were recorded (Fig. 3). The spectra were deconvoluted into contributions of Al^{IV} and Al^{VI} (Table 3). The higher the starting concentration $[Al]_0$, the higher the content of octahedral Al. Note that the aluminium contents of the samples taken out at pH 3 are lower than those of the samples prepared at a higher final pH. For some samples, a small contribution of a resonance between 30 and 35 ppm is noted, which is due to distorted four-coordinated or five-coordinated Al species [33,35,36]. The absolute amount of tetrahedral Al depends only weakly on the aluminium content. In contrast, the amount of Al^{VI} increases strongly with the aluminium content of the ASA.

The deposition of aluminium on silica will now be discussed as a function of the pH and the aluminium content. The synthesis of ASAs starts with the addition of aluminium nitrate to the urea-containing suspension of the silica aerogel. A hexa-aqua aluminium complex $[Al(H_2O)_6]^{3+}$ is formed, which hydrolyzes according to

$$[Al(H_2O)_6]^{3+} \leftrightarrows [Al(H_2O)_5(OH^-)]^{2+} + H^+ \quad (4)$$

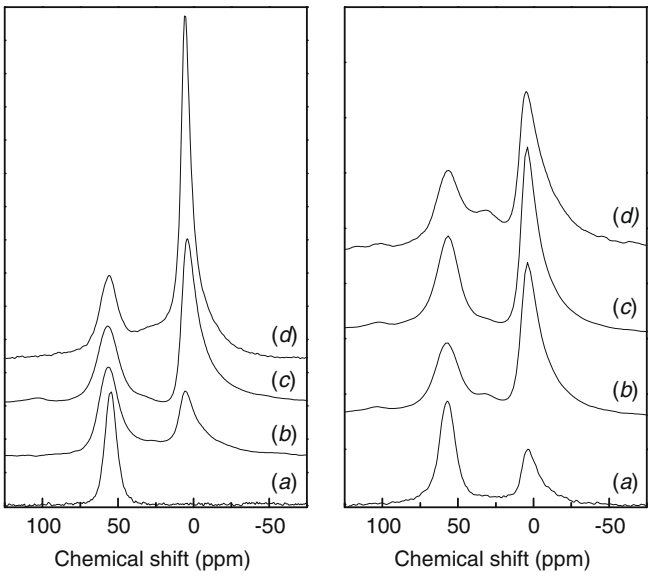

Fig. 3. ^{27}Al NMR spectra of dried ASAs as a function of the aluminium concentration following the completion of urea decomposition (left) and taken out at a pH of 3 (right) with targetted alumina contents of 5 wt% (a), 10 wt% (b), 15 wt% (c) and 20 wt% (d). Note that the actual alumina concentrations in the samples taken out at pH 3 deviate from the targeted concentrations.

Table 3
Coordination of aluminium in dried and calcined ASAs. The values represent the deconvoluted fractions of Al ions in Al^{IV} ($\delta \approx 54$ ppm), Al^{V} ($\delta \approx 30$–35 ppm) and Al^{VI} ($\delta \approx 0$ ppm) coordination.

Sample	393 K			773 K			1073 K		
	Al^{IV}	Al^{V}	Al^{VI}	Al^{IV}	Al^{V}	Al^{VI}	Al^{IV}	Al^{V}	Al^{VI}
ASA(5/95)	100	0	0	60	0	40	48	7	45
ASA(10/90)	50	6	44	44	14	42	50	8	42
ASA(15/85)	35	0	65	45	11	43	38	17	45
ASA(20/80)	24	6	70	30	16	54	26	14	60
ASA(5/95,3)	57	2	38	57	0	43	56	0	44
ASA(10/90,3)	35	4	61	45	2	53	48	4	48
ASA(15/85,3)	40	0	59	40	6	54	45	4	51
ASA(20/80,3)	24	16	60	42	10	48	41	22	37
ASA(5/95,cogel)	100	0	0	57[a]	4[a]	39[a]			
ASA(5/95,fumed)	52	8	40	30	18	52			
ASA(5/95,F)	100	0	0	92	0	8			
ASA(20/80,DA)	80	0	20	47[b]	10[b]	43[b]			

[a] Calcined at 923 K.
[b] Calcined at 823 K.

explaining the strong pH decrease. The initial pH decrease becomes more pronounced with higher $[Al]_0$ (Fig. 1). At low pH, further hydrolysis of the aluminium complexes is limited. The temperature of the suspension is raised in region I and urea decomposition commences above 343 K. As a result, the pH increases in region II. For ASA(5/95), the pH increased strongly in region II. With increasing $[Al]_0$, however, an initial strong pH increase was followed by a more gradual increase of pH with synthesis time. The initial increase is due to the establishment of a new equilibrium between the various charged Al species after the start of urea decomposition. The relatively slow increase at higher $[Al]_0$ comes from the buffering effect from the continuous hydrolysis of the solvated Al^{3+} through

$$[Al(H_2O)_6]^{3+} + OH^- \rightarrow [Al(H_2O)_5(OH^-)]^{2+} + H_2O \quad (5)$$

As this buffering effect becomes smaller at lower $[Al]_0$, a more pronounced pH increase with synthesis time is noted.

As follows from the investigation of the synthesis of ASA(5/95), a substantial amount of Al is grafted in region II (pH 3). All Al is

grafted below pH 4. In order to account for the deposition of aluminium species on silica below pH 3, electrostatic interactions and hydrolytic adsorption should be considered. Electrostatic interactions between the positively charged metal-aquo complexes and their hydrolyzed form(s) with a negatively charged silica surface should, however, not be important under these conditions. Although the point of zero charge of silica is 2, the development of negative charge on its surface is very small below pH 6 [23]. Thus, the contribution of electrostatic interactions should be minor. For pH < 2, as is initially the case for the synthesis with high $[Al]_0$, the silica surface is positively charged, completely precluding such interactions. Alternatively, deposition can proceed via hydrolytic adsorption. This involves the condensation between partially hydrolyzed aquated metal ions with the hydroxyl groups of metal oxides [41]. The dominant Al solution species at pH 3 are sixfold coordinated $Al(H_2O)_6^{3+}$ and $Al(H_2O)_{6-x}(OH)_x^{3-x}$ (x = 1–2). Fig. 4 summarizes the reactions of $Al(H_2O)_5(OH)^{2+}$ with silanol groups at relatively low $[Al]_0$. Initially, hydrolytic adsorption results in a grafted octahedral Al^{3+} species (structure *2*). This species can further hydrolyze to structure *3* and a second condensation reaction with a proximate silanol group becomes possible. The resulting grafted Al species (structure *4*) is tetrahedrally coordinated. This structure was earlier proposed by De Boer [5] and Danforth [56] for the reaction between silica and aluminium ions under acidic conditions. De Boer also postulated the reaction of an $Al_2(OH)_6$ species with one silanol group to form a ≡SiO–$Al_2(OH)_5$ species. Tamele [4] further proposed the reaction of hydrolyzed Al^{3+} species carrying three hydroxyl groups with three silanol groups on the surface, but such condensed species should not exist under these relatively acidic conditions.

Fig. 4 explains the changes in the aluminium coordination following the increase of the pH. At pH 3, already a substantial amount of Al (4.3 wt% Al_2O_3) is grafted onto the silica surface. The contribution of Al^{IV} (Al^{VI}) is 60% (40%). These species are represented by structures *2* and *4*, respectively. The reaction from structures *2* to *4* implies that OH^- is used to hydrolyze not only the aluminium-aquo complexes in the solution, but also grafted Al^{VI}. At the point where the majority of aluminium species have been hydrolyzed, the pH increases strongly due to further release of OH^- from urea. This defines the start of region III. The remaining Al species are deposited on the surface below pH 4. The dominant species in the solution between pH 3 and 4 should still be sixfold coordinated Al, although some Al_{13} complexes may be present as well. The Al coordination in ASA(5/95,4) already indicates that part of the initially grafted monopodal Al^{VI} species (structure *2*) have transformed into bipodal Al^{IV} species (structure *4*). The sample obtained after complete synthesis contains only Al^{IV} species, which is attributed to the further hydrolysis and condensation of all grafted Al^{VI} complexes with silanol groups during the further increase of the pH to its final value of 6.5 (region IV). Thus, condensation reactions between $Al(H_2O)_5(OH)^{2+}$ and silanol groups result in the formation of monopodal Al^{VI} species, which are then further converted upon base-catalyzed hydrolysis and condensation to bipodal Al^{IV} species. It is also possible that some of the grafting occurs via the condensation of $Al(H_2O)_4(OH)_2^+$ with two silanol groups. If during the deposition of aluminium on silica, each Al^{3+} reacts with two silanol groups, one would expect a maximum of 6.5 wt% Al_2O_3 as bipodal Al^{IV} species for this silica aerogel. Indeed, samples prepared at a higher aluminium content contain octahedral Al. The amount of Al^{IV} species in the final dried samples which varies slightly, that is 5.1 wt% Al_2O_3 for ASA(5/95,393), 6.1 wt% for ASA(10/90,393), 5.1 wt% for ASA(15/85,393) and 4.2 wt% for ASA(20/80,393), remains below the predicted maximum of 6.5 wt%. The distribution in Al coordination can be compared with those of the solids extracted at pH 3 (Table 2). Similar to ASA(5/95), a substantial fraction of Al has already been deposited on the silica surface in ASA(10/90,3). Part of these Al atoms present as Al^{VI} species at pH 3 change their coordination to tetrahedral during the completion of the synthesis. The final pH of the synthesis of ASA(10/90) is a bit lower than that of ASA(5/95) as more hydroxyl anions were used to hydrolyze Al. For ASA(15/85) and ASA(20/80), the amount of Al^{IV} decreases. A considerably smaller fraction of the total amount of Al in the synthesis mixture is grafted at pH 3 at this higher Al content. It is then interesting to determine under what conditions the remaining Al species are grafted. When the regular amount of urea was used in the preparation of ASA(20/80), the alu-

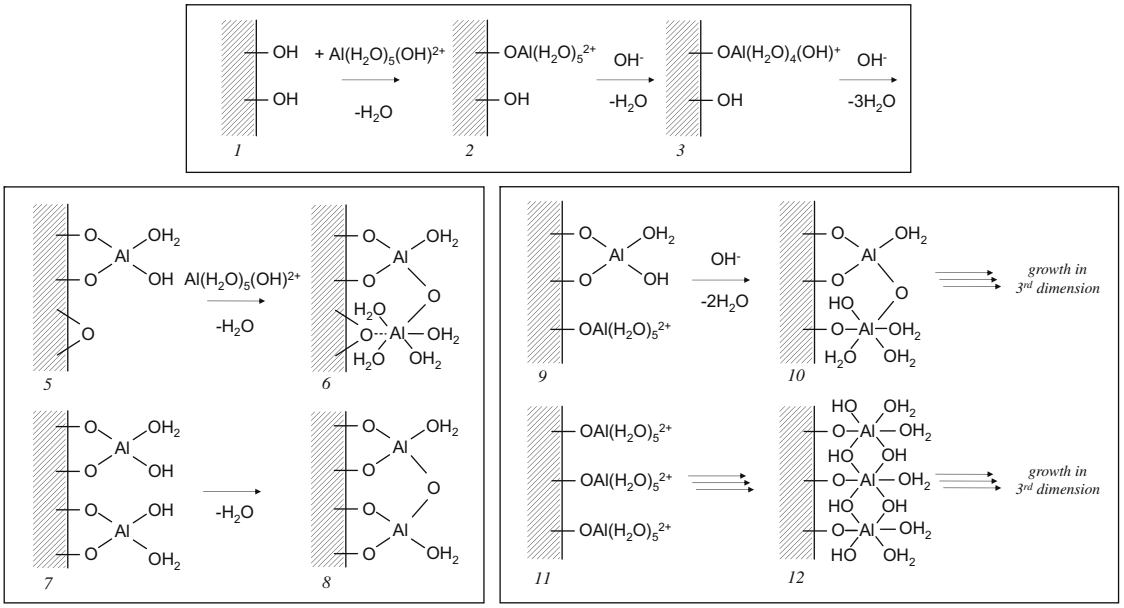

Fig. 4. Schematic representation of the grafting of partially hydrolyzed aluminium ions on silanol groups (*1*) resulting in monopodal (*2*) and bipodal (*4*) aluminium ions; the grafting of partially hydrolyzed aluminium ions to already grafted aluminium (*5* → *6*) and the condensation of hydroxyl groups of promixate bipodal surface aluminium (*7* → *8*) and condensation reactions between grafted bipodal and monopodal aluminium and proximate monopodal aluminium to polymeric forms of aluminium.

mina content was limited to 16 wt% at a final pH of 3.3. When the final pH was increased to 5.5 by using a higher initial urea concentration of 1.1 M, the desired final loading was obtained. Thus, for pH < 3 about 10 wt% Al_2O_3 is grafted, for 3 < pH < 3.3 a further 6 wt% and, for pH > 3.3, the remaining amount of aluminium. These results suggest that most of the deposition of Al takes place below pH 4, even for the most aluminium-rich composition.

On the basis of the Al^{IV} content in ASA(10/90,3) of 3.6 wt%, we calculate that the remaining silanol groups can in principle accommodate an additional 6 wt% Al^{VI} species. The amount of Al^{VI} species in the solid at this stage of the synthesis is 5.4 wt%. However, it is then difficult to see how the amount of Al^{IV} species can increase to 6.1pH wt% after a further increase of pH to 5.5. A reasonable explanation is the condensation between an already grafted Al^{IV} species with aluminium species in the solution. The resulting Al^{VI} species should be more loosely bonded and may for instance interact with a surface siloxane bridge. This deposition reaction is shown in Fig. 4 (structures *5* → *6*). A consequence is that part of the silanol groups remain available for the formation of bipodal Al^{IV} species upon further hydrolysis at a later stage of the synthesis process. This explanation is not unreasonable, because it is well known that the rate of homocondensation between hydrolyzed Al species is higher than the rate of condensation between silanol and aluminol groups [17]. Moreover, the grafting of $Al(H_2O)_5(OH)^{2+}$ on vicinal silanol groups should be unfavourable because of the charge repulsion between the grafted species. Another indication is that the amount of Al^{IV} in ASA(10/90) is close to the maximum predicted value of 6.5 wt%. In some cases, a small amount of distorted Al^{IV} or Al^{V} species are observed and, tentatively, these are attributed to condensation between proximate bipodal Al^{IV} species, giving structure *8* (Fig. 4) which can be considered as distorted tetrahedral Al. Upon a further increase of $[Al]_0$, the amount of Al^{IV} species in the interrupted and final samples decreases. This can be understood in terms of an increased formation of the grafted Al^{VI} species despite the resulting charge repulsion. Further reactions that can take place are those between monopodal Al^{VI} species and bipodal Al^{IV} species (Fig. 4, structures *9* → *10*). Obviously, condensation reactions between the grafted surface Al species and Al in the solution should also be considered at higher $[Al]_0$. Such reactions may lead to the growth of a polymeric aluminium hydroxide phase over the silica surface which may extend in the third dimension as would occur if further Al is grafted on top of structures *10* and *12*.

In summary, the grafting of aluminium species on silica takes place via a hydrolytic adsorption involving condensation reactions between silanol groups and hydrolyzed Al complexes from the solution at relatively low pH. At low $[Al]_0$, monopodal Al^{VI} species are formed which then further condense with proximate silanol groups to bipodal Al^{IV} species when the pH is increased. An increase of $[Al]_0$ reduces the amount of the grafted Al^{IV} species to some extent and leads to the presence of Al^{VI} species on the silica surface, which most likely have reacted with surface Al. At higher aluminium concentration, a polymeric aluminium hydroxide network is formed which may extend into the third dimension. The majority of Al species deposit at relatively low pH where grafting via heterolytic and homolytic adsorption is dominant over precipitation.

To validate the role of the surface hydroxyl group density in the deposition process, a further ASA synthesis was carried out with a fumed silica. The fumed silica has a lower hydroxyl density (1.2 OH/nm^2) than the Sipernat-50 silica (4.1 OH/nm^2). The aluminium loading of ASA(5/95,fumed) is somewhat lower at 4.2 wt% Al_2O_3 compared to that of ASA(5/95). The final pH values of the two syntheses (Table 2) are very similar. Fig. 5 shows the ^{27}Al NMR spectrum of dried ASA(5/95,fumed). This ASA contains five- and six-coordinated Al next to four-coordinated Al. Thus, at a lower surface hydroxyl concentration fewer sites are available for the grafting of aluminium to bipodal Al^{IV} and a larger part of the deposition takes place via condensation reactions with aluminium species already grafted to the surface. Indeed, the Al^{IV} content of 2.1 wt% in ASA(5/95,fumed) corresponds well to the expected maximum value of 2 wt% based on the hydroxyl density of the fumed silica.

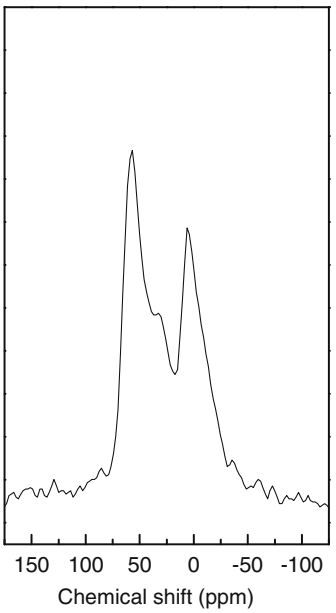

Fig. 5. ^{27}Al NMR spectrum of ASA(5/95, fumed). The hydroxyl density of the fumed silica starting material is substantially lower (1.2 OH/nm^2) than that of the silica aerogel (4.1 OH/nm^2).

3.2. Calcination

Prior to their use as catalysts, ASA precursors are typically calcined at temperatures around 773 K to bring about the desired acidity. As will be shown below, these ASAs display the typical catalytic activity of industrial ASAs in alkane hydroconversion. Since calcination at 1073 K afforded more active catalysts, a detailed comparison of calcination at 773 and 1073 K was made. Firstly, the coordination of aluminium in the calcined ASAs will be compared by ^{27}Al NMR spectroscopy. The stepwise calcination up to 773 K will be investigated in more detail for a few samples. ^{29}Si NMR spectra at varying loadings will be compared. Secondly, transmission and secondary electron microscopies were employed to study the spatial distribution of aluminium on the silica surface. Finally, the presence and composition of the segregated alumina phase were investigated by two methods of NMR, namely rotational resonance ^{27}Al NMR to probe the proximity of octahedral to tetrahedral Al nuclei as is typical found in transition aluminas and ^{27}Al NMR after ammonia adsorption to distinguish octahedrally coordinated Al atoms in a mixed silica-alumina phase from those in separate alumina domains.

3.2.1. Coordination environment of aluminium in calcined ASAs

Fig. 6 shows the ^{27}Al NMR spectra of the calcined ASAs. In comparison with those of the dried precursors, considerable changes in the chemical environment of aluminium are apparent. Firstly and foremost, the major part of the redistribution of the coordination environment of aluminium occurs upon calcination at 773 K (Fig. 6a). The changes after calcination at 1073 K (Fig. 6b) are relatively minor. Calcination at 773 K converts part of the four-coordinated Al in ASA(5/95) and ASA(10/90) to six-coordinated Al,

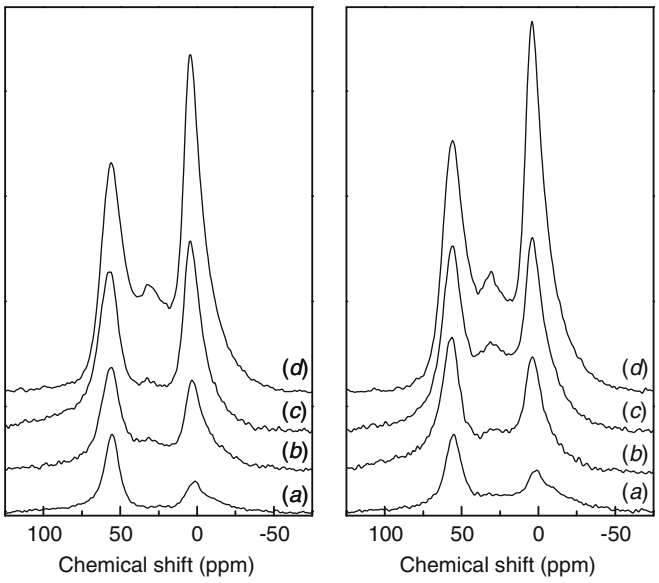

Fig. 6. ^{27}Al NMR spectra of ASA(5/95) (a), ASA(10/90) (b), ASA(15/85) (c) and ASA(20/80) (d) calcined at 773 K (left) and 1073 K (right).

whereas the reverse holds for ASA(15/85) and ASA(20/80). A preliminary explanation is one in terms of the formation of a separate transition alumina phase on the surface. The fraction of tetrahedral aluminium in spinel-structure transition aluminas is between 25 and 37% [57]. At low alumina content, the appearance of octahedral Al points to the agglomeration of isolated Al via the formation of Al-O-Al bonds. The changes at higher aluminium concentrations can be attributed to dehydration of the polymeric aluminium oxohydroxide network in which octahedral Al is dominant into a transition alumina phase. The corresponding spectra of the calcined ASAs prepared at final pH 3 (Fig. 7) show similar trends, albeit that the changes are now less pronounced. Brønsted acidity induced by calcination is most likely due to the diffusion of aluminium atoms into the silica surface, where it substitutes Si^{4+} and induces a negative charge at the surface which requires compensation. Although tetrahedral Al at the surface cannot be distinguished from tetrahedral Al in the surface, the current thinking is that only very few such substitutions exist in the silica network [31].

Secondly, the presence of a weak signal between 30 and 35 ppm in some of the ^{27}Al NMR spectra is noted. The amount of such species increased with the aluminium concentration. This peak stems either from tetrahedral Al shifted by a strong quadrupolar distortion or from a five-fold coordinated Al species (Al^{V}). Multiple Quantum MAS NMR measurements can distinguish between these two coordination states by separating the quadrupolar and chemical effects on the chemical shift. To verify the assignment to five-coordinated Al for these ASAs, MQMAS NMR measurements for ASA(5/95,1073) and ASA(15/85,1073) were recorded (see Supporting Information). These data unequivocally show the presence of five-coordinated Al at an isotropic chemical shift around 30 ppm. The contribution of these aluminium species increased with the aluminium concentration. The single pulse ^{27}Al NMR spectra were deconvoluted into lineshape components attributed to Al^{IV}, Al^{V} and Al^{VI}. Typically, deconvolution required two Gaussian components to fit the lineshape of Al^{VI}; the Al^{V} and Al^{IV} signals were fitted with single Gaussian lineshapes. The results for a large set of ASAs are listed in Table 3.

To understand the redistribution upon calcination, the evolution in the aluminium coordination of ASA(5/95) as a function of temperature was followed. ASA(5/95) was chosen because the surface of the dried precursor is expected to contain quite uniformly distributed grafted Al^{IV} atoms. As the surface density of Al most likely plays a role in the redistribution process, the calcination of an ASA with a substantially lower Al content, ASA(1/99), prepared in a similar manner as ASA(5/95) was investigated as well. Fig. 8 shows NMR spectra of the stepwise calcination. Calcination at 473 K results in the appearance of an octahedral signal in ASA(5/95) with a contribution of about 28% (Fig. 8a). Its contribution grows further after calcination at 573 K and then remains constant up to a calcination temperature of 773 K. In comparison, the grafted Al^{IV} species in ASA(1/99) are stable at least until calcination at 573 K and further calcination at 773 K and 1073 K brings about only a weak and broad signal around 0 ppm (Fig. 8b).

The difference between ASA(1/99) and ASA(5/95) indicates that the agglomeration of the grafted Al^{IV} species on the silica surface strongly depends on their surface density. When the surface coverage with bipodal Al^{IV} is high, condensation reactions take place be-

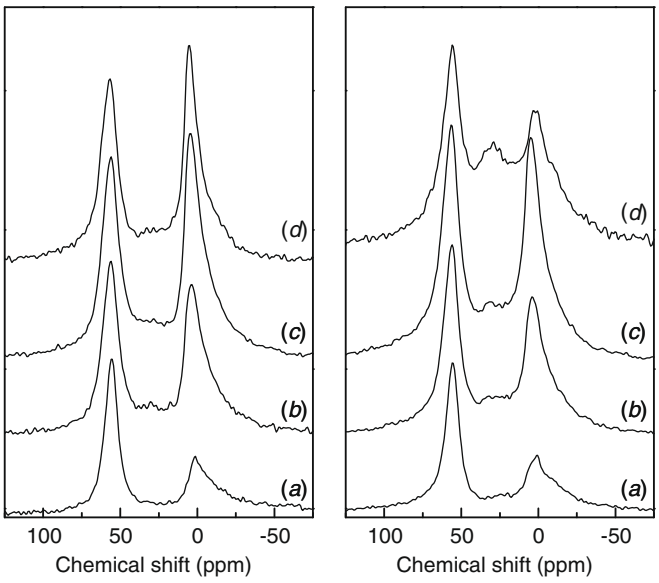

Fig. 7. ^{27}Al NMR spectra of ASA(5/95,3) (a), ASA(10/90,3) (b), ASA(15/85,3) (c) and ASA(20/80,3) (d) calcined at 773 K (left) and 1073 K (right).

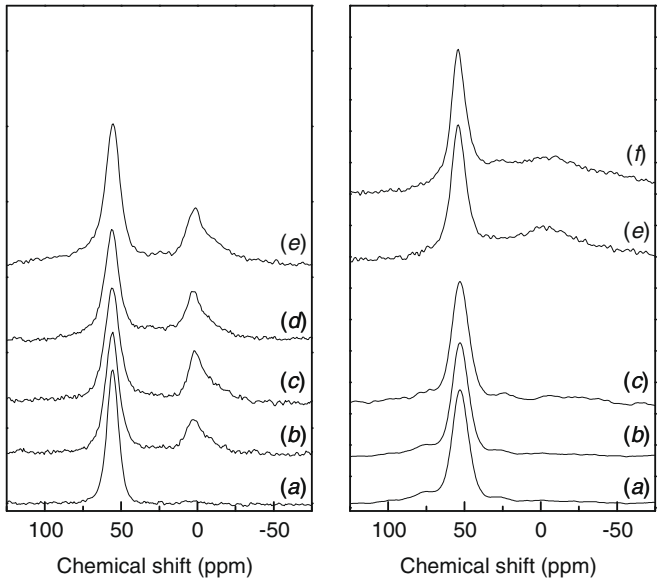

Fig. 8. ^{27}Al NMR spectra of ASA(5/95) (left) and ASA(1/99) (right) after calcination at 393 K (a), 473 K (b), 573 K (c), 673 K (d), 773 K (e) and 1073 K (f).

tween the Al^{IV} already at quite low temperature. These reactions should involve the rupture of the bonds with the silica surface and it can be envisioned that associated water plays a role in the rehydrolysis of the Si–O–Al bonds. On the other hand, when the grafted Al^{IV} becomes more diluted, they are thermally stable and do not agglomerate, even when the material is calcined at 1073 K.

3.2.2. High-power decoupled ^{29}Si NMR spectroscopy

Fig. 9 shows the proton-decoupled MAS ^{29}Si NMR spectra of two ASAs with nominal alumina contents of 5 and 15 wt% and calcined at 773 K prepared in a similar manner. The ^{29}Si NMR chemical shift is mainly affected by the chemical composition of the first and second coordination. The spectra are made up of two overlapping contributions from silicon atoms with tetrahedral oxygen coordination. The dominant resonance at −107 ppm is due to ^{29}Si with Q^4 coordination, *i.e.* four silicon atoms in the second coordination sphere. The asymmetric lineshape indicates the contribution of a resonance at −97 ppm, which belongs to Q^3-type silicon sites with three silicon atoms and either a hydrogen or aluminium atom in the second coordination sphere. The ^{29}Si NMR lineshape for the sample with the low and high alumina concentration is practically the same. Lineshape deconvolution indicates similar Q^3 fractions of 16 ± 1%. The fact that the Q^3 fraction does not increase at increasing Al content above 5 wt% Al_2O_3 suggests that above a certain Al content, additional aluminium is not built into the aluminosilica phase anymore, but into a separate alumina phase. This result also indicates that extensive diffusion of aluminium into the silica should not occur during calcination at 773 K.

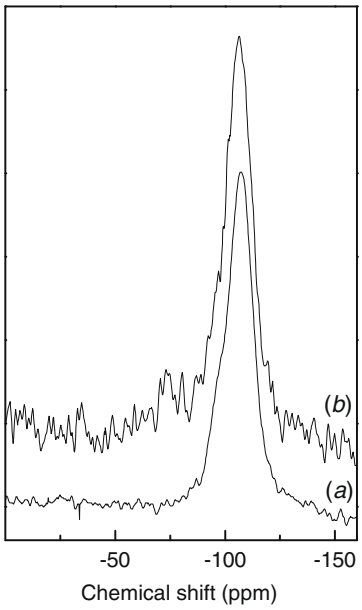

Fig. 9. ^{29}Si NMR spectra of two amorphous silica-aluminas prepared in a manner similar to that of ASA(5/95,773) (a) and ASA(15/85,773) (b).

3.2.3. Homogeneity of the grafting process

To obtain an impression about the homogeneity of the surface distribution of aluminium, scanning electron micrographs of the block faces were recorded for ASA(5/95,773) and ASA(20/80,773). Fig. 10 shows that the aluminium density differs slightly between various silica particles. Heterogeneity on the scale of the silica grains should be due to the differences in the hydroxyl density, which is a reasonable explanation as the parent silica was prepared by spray drying. In passing, we note that the substantial difference between ASA(5/95,773) and ASA(20/80,773) with open and compact morphologies, respectively, must have arisen during post-processing steps (filtration and calcination) of the materials.

For some ASAs the distribution of aluminium was analyzed in more detail by scanning transmission electron microscopy using line scans over areas of 5 × 5 μm. The samples in this case were Pd-loaded catalysts to be used for the alkane hydroconversion activity measurements. Fig. 11 shows representative results for ASA(5/95,1073), ASA(20/80,773) and ASA(20/80,3,1073). For ASA(5/95,1073), regions are observed where aluminium is rather uniformly distributed, *e.g.* position 2 in Fig. 11a, as follows from the linear relation between the signals of the Si and Al K edges. On the other hand, regions with a less homogeneous Al distribution were also observed. The variance in aluminium content per particle is exemplified for two particles in ASA(5/95,1073) with average values of 5.3 wt% (covariance 11.6%) and 5.9 wt% (covariance 6.1%). Compared to ASA(20/80,773), however, the distribution is rather homogeneous. The aluminium distribution in ASA(20/80,773) varies quite strongly with the position. The differences between particles are also pronounced, *e.g.* two different particles contained 20.8 and 24.1 wt% Al_2O_3. The less uniform aluminium distribution with increasing aluminium concentration agrees with the deposition model discussed above. A considerable part of aluminium in ASA(20/80) reacts with initially grafted Al species. This may give rise to local concentration gradients of surface Al. The final pH of the synthesis of ASA(20/80) is 5.5, which means that some precipitation of pseudo-boehmite might have taken place. This is further supported when the data for ASA(20/80,3,1073) are taken into account. In the case that the deposition–precipitation process was stopped at pH 3, aluminium was found to be distributed quite homogeneously over the surface. Moreover, the alumina contents of two particles (16.8 and 16.9 wt% Al_2O_3) are quite similar. Grafting of aluminium to the silica surface and to

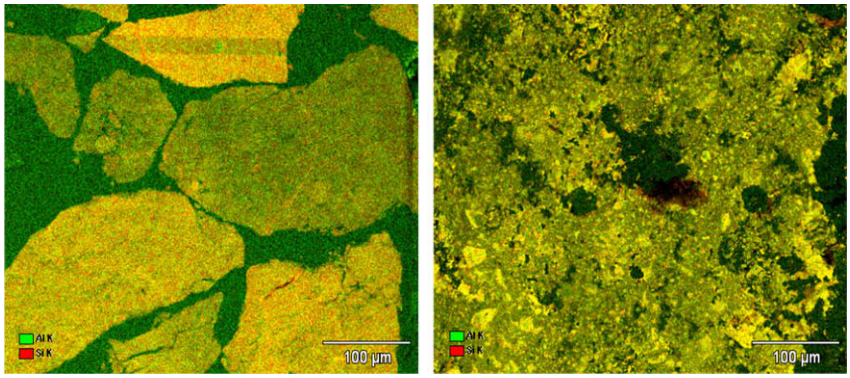

Fig. 10. SEM/EDS micrographs of block faces of ASA(5/95,773) and ASA(20/80,773) (red: regions rich in silicon; green: regions rich in aluminium). (For interpretation of the references to colour in this figure legend, the reader is referred to the web version of this article.)

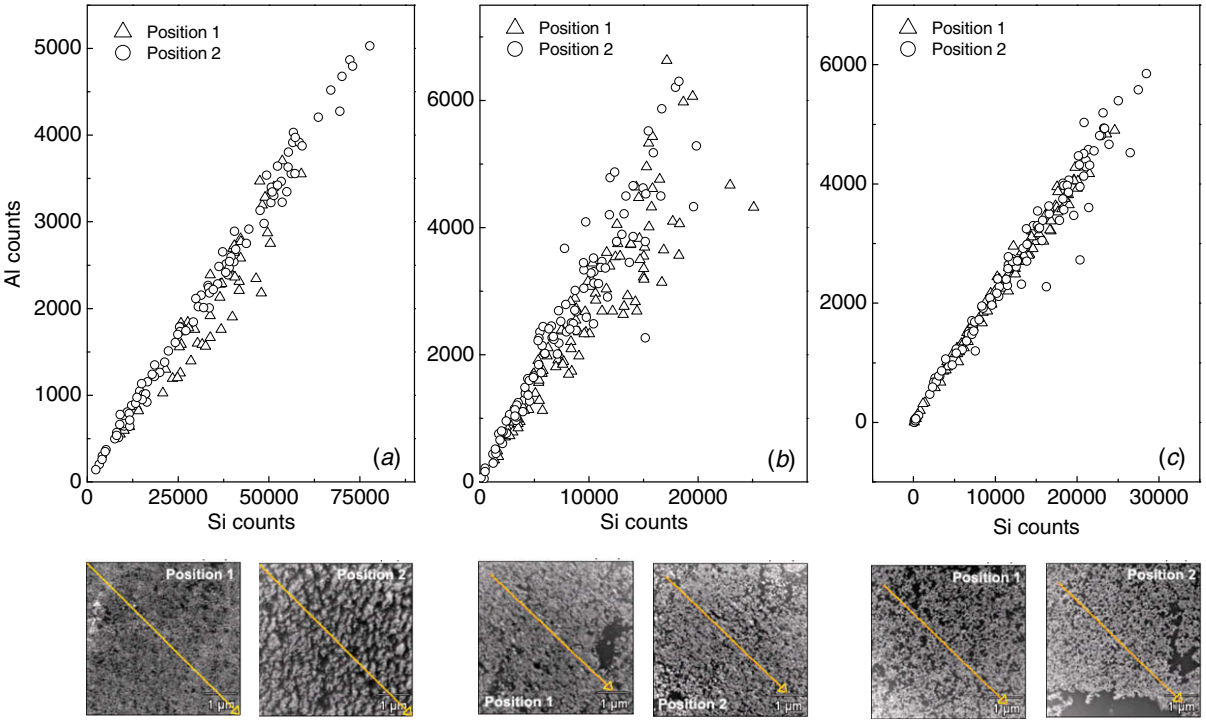

Fig. 11. Si and Al counts across a diagonal line scan of a section of 5 × 5 μm measured by scanning TEM/EDS in ASA(5/95,1073) (a), ASA(20/80,773) (b) and ASA(20/80,3,1073) (c), each at two different positions. The corresponding electron micrographs are given below.

already grafted Al species is the dominant process under these conditions and results in a homogeneous Al distribution. In summary, the electron microscopy analyses show that the deposition of Al occurs rather homogeneously on the local scale for pH < 3. At higher pH, there is much more variation in the aluminium content, which is due to the competition of precipitation with the grafting reactions. On the scale of the silica particles inhomogeneities are noted, presumably because of variations in the hydroxyl densities of the silica grains.

3.2.4. Distribution of Al in a mixed silica-alumina phase and alumina domains

The different changes in Al distribution following calcination for ASAs prepared at low and high aluminium contents suggest that a fraction of aluminium is converted into domains of alumina. For a commercial ASA with a higher aluminium content, the presence of γ-Al_2O_3 is evident in transmission electron micrographs by the observation of nanometer-sized crystalline particles with the typical *d*-spacings of γ-alumina. No evidence for the presence of γ-Al_2O_3 was found in the set of HDP ASAs, suggesting that such particles, if at all present, should be very small. The flexibility of the coordination of octahedral Al in ASAs can be used to distinguish between Al in alumina domains and Al in a mixed silica-alumina phase [31,37]. For example, the coordination of octahedral Al in γ-alumina does not change upon exposure to ammonia. Part of octahedral Al in ASAs change their coordination and are therefore considered to be part of the mixed phase. Williams et al. [31] assumed that non-flexible Al^{VI} in ASAs is present as γ-Al_2O_3 domains (tetrahedral Al:octahedral Al = 3:7). With this assumption, the distribution of aluminium over γ-Al_2O_3 and a mixed silica-alumina phase can be calculated. The assumption that alumina occurs as γ-Al_2O_3 does not introduce a large error as the fraction of Al^{IV} in typical transition aluminas varies between 27% and 35% [57].

Before discussing NMR data before and after ammonia adsorption, we first verified whether the HDP ASAs contain the suspected transition alumina phase. To distinguish between tetrahedrally coordinated aluminium atoms in the mixed silica-alumina and alumina phases in ASA, we make use of the fact that Al atoms in a pure silica-alumina phase have only Si neighbours, whereas the alumina phase contains neighbouring tetrahedral and octahedral Al atoms at typical separation of 3 Å. At such distance, Al nuclei have a homonuclear dipolar coupling with a constant of about 140 Hz. In principle, this ^{27}Al–^{27}Al coupling between octahedral and tetrahedral Al atoms could be used as a distinguishing feature between Al in the mixed silica-alumina and alumina phase. However, the same magic-angle spinning that is required for ^{27}Al NMR line narrowing also suppresses the ^{27}Al–^{27}Al coupling, in general. Fortunately, an exceptional situation arises, if the sample-rotation rate matches the peak separation. Then, constructive interference occurs between the periodic modulations in the dipolar Hamiltonian by the sample rotation and chemical-shift difference, and spin polarization may be exchanged between the coupled nuclei. Such special dipole-coupling effect when the sample rotation matches the peak separation is called rotational resonance (R^2) and it has been employed to measure the coupling constants of isolated spin 1/2 pairs, such as ^{13}C–^{13}C for distance measurements in solid organic compounds [58]. For quadrupolar nuclei, like ^{27}Al with spin 5/2, the case becomes complicated by cross-interference with the quadrupolar coupling, as well as the possible pulse-selectivity artefacts. In addition, the ^{27}Al nuclei in the alumina phase do not occur as isolated pairs, and thus multispin effects arise. Therefore, the polarization transfer is expected to proceed in a spin-diffusive, rather than in an oscillatory way.

Aiming at a semi-quantitative NMR tool, we have empirically tested the R^2 technique for ^{27}Al NMR of pure γ-alumina with neighbouring tetrahedral and octahedral Al, on the one hand, and zeolite HZSM-5 with isolated tetrahedral Al only, on the other hand. Fig. 12 shows the polarization recovery of the tetrahedral ^{27}Al nuclei after a selective pulse scheme which alternatingly inverts the polarization of Al spins resonating at either 56 or

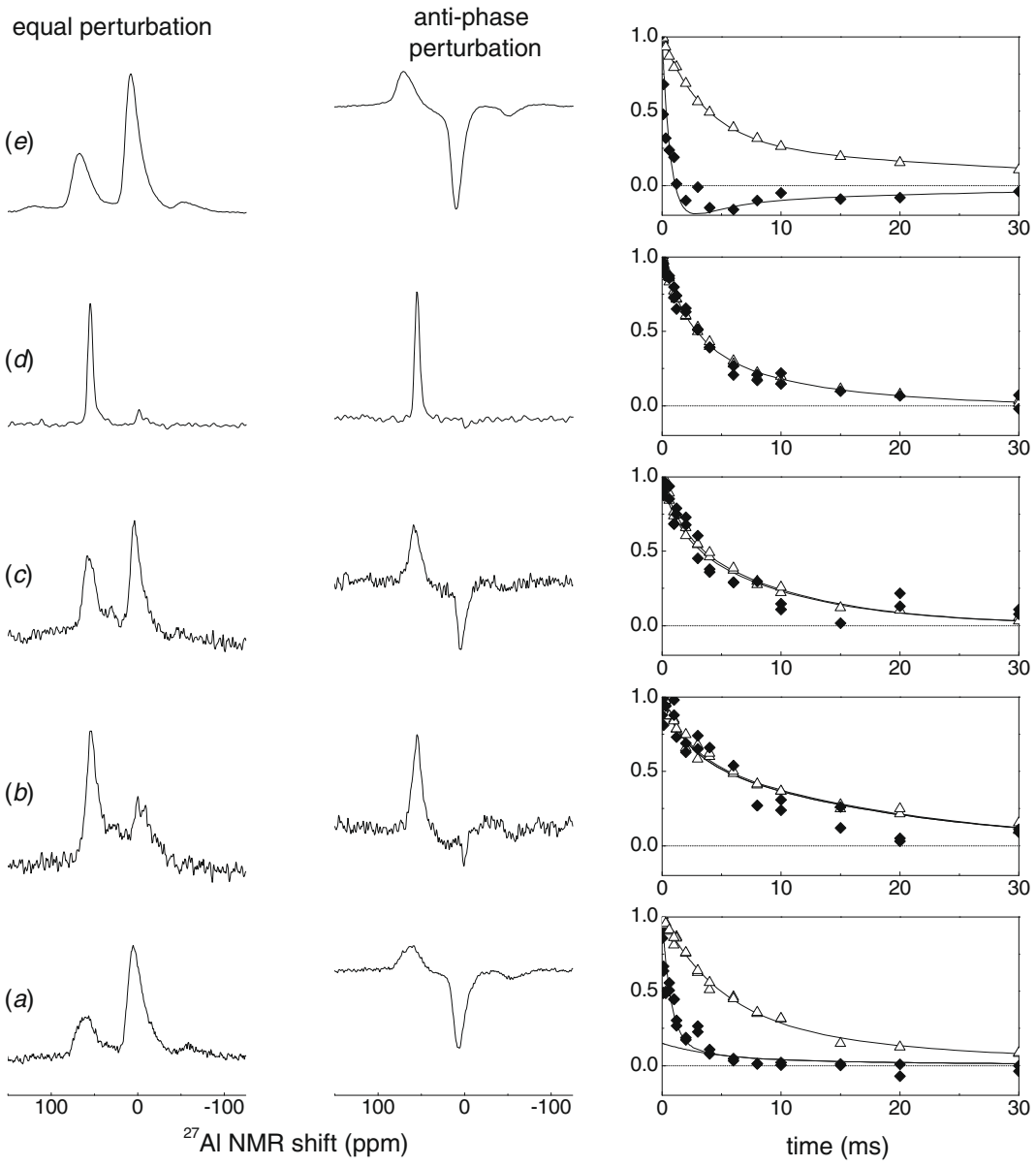

Fig. 12. ^{27}Al spin exchange between octahedral and tetrahedral Al in ASAs: (a) ASA(55/45), (b) ASA(20/80,1073) and (c) ASA(5/95,1073). For comparison the upper part of the figure shows the results for (d) zeolite HZSM-5 (Si/Al = 20) and (e) γ-Al_2O_3. The left column shows the ^{27}Al NMR spectra with equally excited tetrahedral and octahedral Al nuclei. The centre column reflects the anti-phase perturbation prior to mixing time. The right column shows the decay of the tetrahedral Al signal at 56 ppm (♦) during the mixing time as the combined result of spin exchange in the alumina phase and spin-lattice relaxation. For comparison spin-lattice relaxation has also been measured separately (△).

6 ppm. Such pulse scheme yields anti-phase polarization, *i.e.* the tetrahedral and octahedral Al spins are prepared with opposite polarization. In the subsequent 'mixing time' the neighbouring tetrahedral and octahedral Al alumina are given the opportunity to exchange polarization. The polarization of the isolated Al sites in the zeolite only changes under the influence of spin-lattice relaxation. This relaxation, which affects the ^{27}Al spins in alumina as well, can be independently measured in control experiments with a non-selective polarization perturbation of both the tetrahedral and octahedral ^{27}Al nuclei. In all cases, the sample-rotation rate was matched to the chemical-shift difference (∼7.5 kHz).

As can be seen in Fig. 12d and e, alumina and zeolite HZSM-5 behave markedly different. For the zeolite the rate at which the tetrahedral signal at 56 ppm recovers after the selective pulse is the same as after the nonselective pulse. For γ-Al_2O_3, in contrast, the recovery of the tetrahedral Al polarization after the anti-phase polarization perturbation of the tetrahedral and octahedral Al spins strongly differs from the background relaxation. This is a consequence of the R^2 effect, which induces polarization exchange between the octahedral and tetrahedral Al nuclei, and yields a fast redistribution of the perturbed polarization over the two Al types in alumina before the whole system of octahedral and tetrahedral Al relaxes back to thermal equilibrium, as a homogeneously polarized ensemble.

Given the different R^2 behaviours of tetrahedral Al in alumina and zeolite HZSM-5, the technique was employed as a semi-quantitative tool for discriminating between tetrahedral Al in the alumina and the mixed silica-alumina phases in ASA. Fig. 12a–c shows the results for ASA(5/95,1073), ASA(20/80,1073) and a commercial ASA with an nominal Al_2O_3 content of 55 wt%, here denoted by ASA(55/45). The commercial ASA contains γ-alumina as evidenced by TEM. It is immediately clear from this figure that

the tetrahedral Al in ASA(5/95) and ASA(20/80) behave as isolated sites without octahedral Al neighbours. This indicates that up to such Al concentrations no predominant alumina phase is present in ASA. ASA(55/45), however, shows faster R^2 exchange than spin-lattice relaxation. The behaviour is in between that of HZSM-5 and γ-Al_2O_3.

To analyze the R^2 curves in more detail and to estimate the alumina fraction in ASA from the bi-component behaviour in the R^2 exchange, we have taken a two-site exchange model for polarization exchange between neighbouring tetrahedral and octahedral ^{27}Al spins in the alumina phase, and extended this with two isolated sites representing ^{27}Al spins in the mixed silica-alumina phase (see Supporting Information). On the basis of this model we have analyzed the recovery curves in terms of a fast R^2 spin-exchange component and a slow background decay, according to

$$I_T(t) = I_T(0)\{A_T \exp(-t_{mix}/\tau_{se}) + 1 - A_T\}R(t_{mix}) \quad (6)$$

with A_T and τ_{se} being the amplitude and characteristic time of the fast decay component caused by spin exchange, respectively. $R(t_{mix})$ is the background decay determined independently from the spin-lattice relaxation after nonselective perturbation. In all cases, the background decays turned out to be well described by a bi-exponential curve of the form

$$R_0(t_{mix}) = I_0'\{A \exp(-t_{mix}/T_{1A}) + B \exp(-t_{mix}/T_{1B})\} \quad (7)$$

with A, B, T_{1A}, and T_{1B} being, respectively, phenomenological fractions and spin-lattice relaxation times. For every alumina and ASA sample measured, the background decays for the tetrahedral and octahedral aluminium nuclei were the same within error, as consistent with the polarization averaging resulting from spin diffusion. The deviation from mono-exponential behaviour need not reflect heterogeneity, since spin-lattice relaxation of quadrupolar nuclei in solid-state NMR can be described intrinsically bi-exponential [59]. According to this model, the relative amplitude A_T of the fast decay components related to the relative number of tetrahedral Al in the alumina phase, as

$$A_T = \kappa \frac{N_{Al_2O_3,T}}{N_{Al_2O_3,T} + N_{AS,T}} \quad (8)$$

with $N_{Al_2O_3}$ and $N_{AS,T}$ being the number of tetrahedral Al sites in the alumina and a mixed silica-alumina phase, respectively. The proportionality constant κ equals $f_{Al2O3,O}(1\text{-}p_O(0)/p_T(0))$ where $f_{Al2O3,O}$ denotes the fraction of octahedral sites in the alumina phase, and $p_O(0)$ and $p_T(0)$ denote the polarization of the octahedral and tetrahedral Al spins and $p_O(0)$ and $p_T(0)$ immediately after the selective perturbation preceding the mixing time. Note that κ and the spin-exchange component vanish, if the octahedral and tetrahedral Al sites are equally perturbed prior to the mixing time t_{mix}. Indeed, this exactly corresponds to the experimental condition to measure the relaxation background decay $R(t_{mix})$ without R^2 exchange. The largest amplitude of the spin-exchange component occurs for perfect anti-phase perturbation, *i.e.* if the initial polarization values of the tetrahedral and octahedral sites have opposite values, $p_O(0) = -p_T(0)$. As for the other parameter $f_{Al2O3,O}$, γ-Al_2O_3 and several other transition alumina types, have a typical octahedral Al fraction of about 0.7. Under these conditions κ reduces to 1.4.

Table 4 summarizes the fit parameters extracted from the R^2 exchange curves in Fig. 12 by the use of Eqs. (6) and (7). Parameters A, B, T_{1A}, and T_{1B} in Eq. (7) were determined independently in separate spin-lattice relaxation experiments. Only $I_T(0)$, A_T and τ_{se} were allowed to vary during fitting of Eq. (6) to the observed R^2 exchange curves for γ-Al_2O_3 and ASA(55/45). The R^2 curve of the latter was measured twice to check the reproducibility of the experiment and analysis. For HZSM-5, ASA(5/95) and ASA(20/80), τ_{se} was fixed to the value 0.86, *i.e.* the characteristic spin-exchange time found for γ-Al_2O_3 and the alumina phase in ASA(55/45). The low amount of Al in ASA(5/95) caused severe scattering of the R^2 exchange data measured with ^{27}Al NMR. The bi-exponential fit to the non-exponential spin-lattice relaxation decays comes with large correlation errors in the fit parameters. For better comparison the more significant weight-average relaxation times $T_{1,av} = [A/T_{1A}+B/T_{1B}]^{-1}$, with A + B = 1, are also given in Table 6. The value $A_T = 1.4$ extracted from the R^2 decay of γ-Al_2O_3 perfectly corresponds to theoretical value for a pure Al_2O_3 (fraction tetrahedral 30%), in combination with perfect anti-phase perturbation of the Al spins prior to the mixing time. This indicates that despite the simplifications in the model such as neglecting the influence of the quadrupolar interaction, the estimated fraction tetrahedral Al atoms in the alumina phase from resonance NMR may be correctly estimated. With the proportionality constant $\kappa = 1.4$, the average value A_T of 0.86 obtained for ASA(55/45) suggests that about 60%

Table 4
Parameters used to fit the model described by Eqs. (6) and (7) to the R^2 exchange and spin-lattice relaxation data.

R^2 exchange			Spin-lattice relaxation			
Sample	A_T	τ_{sd} (ms)	A	T_{1A} (ms)	T_{1B} (ms)	$T_{1,av}$[a] (ms)
γ-Al_2O_3	1.4	0.86	0.67	3.3	29	4.6
HZSM-5	0.0	0.86[b]	0.55	2.2	10	3.6
ASA(5/95,1073)	0.0	0.86[b]	0.35	2.2	18	5.0
ASA(20/80,1073)	0.0	0.86[b]	0.33	1.6	9.9	3.6
ASA(55/45)[c]	0.85	0.83	0.77	4.2	33	5.9
	0.87	0.88	0.77	4.2	33	5.9

[a] Average relaxation time $T_{1,av} = [A/T_{1A} + B/T_{1B}]^{-1}$ are given for comparison.
[b] For HZSM-5, ASA(5/95) and ASA(20/80), τ_{se} was fixed to the value found for γ-Al_2O_3 and ASA(55/45).
[c] The R^2 curve for ASA(55/45) was measured twice and analyzed with the same T_1 relaxation parameters.

Table 5
Distribution of Al in mixed silica-alumina and alumina phases in ASAs calcined at 773 K. NMR spectra recorded before and after exposure to ammonia (indicated by suffix NH_3). Values represent the percentages of the total amount of Al. The nominal Al content (w_{Al2O3}) of both phases is given as well.

Sample	Al coordination			Mixed phase[a]			Alumina domains[b]	
	Al^{IV}	Al^{V}	Al^{VI}	Al^{IV} + Al^{VI}	Interface	w_{Al2O3} (wt%)	Al^{VI}	w_{Al2O3} (wt%)
ASA(5/95)	60	0	40	66	3	3.5	31	1.6
ASA(5/95)-NH_3	66	3	31					
ASA(5/95,3)	57	0	43	100	0	4.3	0	0
ASA(5/95,3)-NH_3	100	0	0					
ASA(20/80)	30	16	54	33	26	12	39	8.0
ASA(20/80)-NH_3	33	26	39					
ASA(20/80,3)	42	19	48	65	6	7.1	29	2.9
ASA(20/80,3)-NH_3	65	6	29					

[a] Mixed phase contains Al^{IV} and Al^{VI} reverted to Al^{IV} after ammonia adsorption (Al^{IV} + Al^{VI}) and Al^{V} after ammonia adsorption (interface).
[b] Alumina domains contain Al^{VI}, whose coordination does not change following ammonia adsorption.

Table 6
Distribution of Al in mixed silica-alumina and alumina phases in ASAs calcined at 1073 K. NMR spectra recorded before and after exposure to ammonia (indicated by suffix NH_3). Values represent the percentages of the total amount of Al. The nominal Al content (w_{Al2O3}) of both phases is given as well.

Sample	Al Coordination			Mixed phase[a]			Alumina domains[b]	
	Al^{IV}	Al^{V}	Al^{VI}	Al^{IV} + Al^{VI}	Interface	w_{Al2O3} (wt%)	Al^{VI}	w_{Al2O3} (wt%)
ASA(5/95)	48	7	45	74	6	4.0	20	1.0
ASA(5/95)-NH_3	74	6	20					
ASA(10/90)	50	8	42	64	12	7.7	24	2.4
ASA(10/90)-NH_3	64	12	24					
ASA(15/85)	38	17	45	44	28	10.9	28	4.2
ASA(15/85)-NH_3	44	28	28					
ASA(20/80)	26	14	60	48	30	15.6	22	4.4
ASA(20/80)-NH_3	48	30	22					
ASA(5/95,3)	56	0	44	87	0	3.7	13	0.6
ASA(5/95,3)-NH_3	87	0	13					
ASA(10/90,3)	48	4	48	66	12	7.0	22	2.0
ASA(10/90,3)-NH_3	66	12	22					
ASA(15/85,3)	45	4	51	59	16	9.1	25	3.0
ASA(15/85,3)-NH_3	59	16	25					
ASA(20/80,3)	41	22	37	59	11	7.0	30	3.0
ASA(20/80,3)-NH_3	59	11	30					
ASA(5/95,cogel)	57	4	39	84	4	4.4	12	0.6
ASA(5/95,cogel)-NH_3	84	4	12					

[a] Mixed phase contains Al^{IV} and Al^{VI} reverted to Al^{IV} after ammonia adsorption (Al^{IV} + Al^{VI}) and Al^{V} after ammonia adsorption (interface).
[b] Alumina domains contain Al^{VI}, whose coordination does not change following ammonia adsorption.

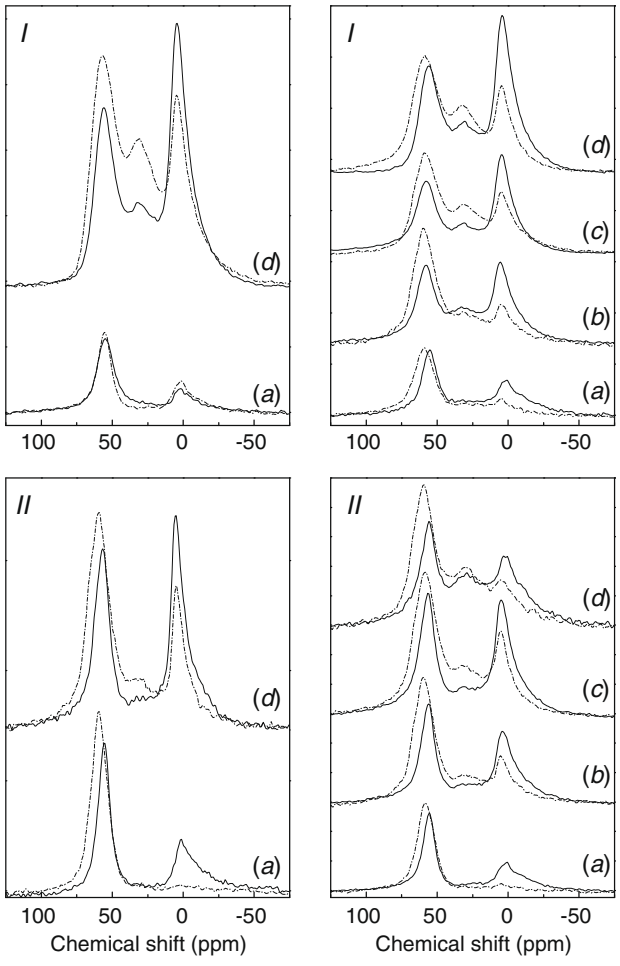

Fig. 13. ^{27}Al NMR spectra of ASAs following full synthesis (I) and until pH 3 (II) calcined at 773 K (left) and 1073 K (right) before (full line) and after (dashed line) ammonia adsorption: ASA(5/95) (a), ASA(10/90) (b), ASA(15/85) (c) and ASA(20/80) (d).

of the tetrahedral Al atoms are located in the alumina phase. The two ASAs prepared by homogeneous deposition–precipitation do not contain octahedral Al near tetrahedral Al. The content of a separate phase with the characteristic presence of octahedral and tetrahedral Al in proximity can therefore be considered to be negligible. Instead, this phase only contains octahedral Al.

Fig. 13 shows then the NMR spectra before and after NH_3 adsorption for the HDP ASAs. The single pulse ^{27}Al NMR spectra were deconvoluted into Al^{IV}, Al^{V} and Al^{VI} contributions and the results are listed in Tables 5 and 6. The initial spectrum of ASA (5/95,773) contains an Al^{IV} signal at 55 ppm and two contributions of Al^{VI} signals around 0 ppm. After dehydration and adsorption of ammonia, the signal of Al^{IV} has slightly grown at the expense of the octahedral Al signal. Thus, a small fraction of the Al^{VI} in ASA(5/95,773) displays flexible coordination. After calcination at 1073 K, the changes are more pronounced. In this case, a small downfield shift of the Al^{IV} signal is observed from 55 to 59 ppm. The changes for the two ASA(5/95,3) samples are much more pronounced. All octahedral Al in ASA(5/95,3,773) reverted to tetrahedral coordination after the adsorption of ammonia. Thus, ASA(5/95,3,773) is a rather pure amorphous silica-alumina sample free of alumina domains. The shift in the Al^{IV} peak position relates to the ligand exchange. With increasing aluminium content, the changes in aluminium coordination become less pronounced. The changes are larger for the complete synthesis ASAs than for the ASAs prepared at final pH 3.

The presence of Al^{VI} atom that cannot be reinserted into the mixed phase points to the presence of very small clusters of aluminium oxide. It should be noted beforehand that some of the six-coordinated Al changes its coordination to a fivefold one upon ammonia adsorption. Further MQMAS NMR measurements are needed to determine whether these Al atoms exhibit distorted tetrahedral coordination or are truly five-coordinated. However, for the present discussion their flexibility will be taken as an argument that they are part of the mixed silica-alumina phase.

The distribution of Al in a mixed silica-alumina phase and alumina domains for a subset of ASAs is presented in Tables 5 and 6. We make use here of the finding by R^2 NMR that octahedral Al nearby enough to tetrahedral Al to consider the presence of a transition alumina phase is absent in the sample with the highest Al content. Thus, the amount of inflexible Al^{VI} corresponds to the amount of a separate aluminium oxide phase. As will be shown below, the amount of Al^{V} after ammonia adsorption represents the

interface between the alumina domains and the mixed phase in line with the conclusion of Williams et al. [31]. Furthermore, Al^V is considered part of the mixed silica-alumina phase. Some general trends will be discussed here. Only at the lowest alumina content, the surface of the ASA prepared at final pH 3 can be considered a pure mixed silica-alumina phase. The absence of octahedral Al after ammonia adsorption shows that ASA(5/95,3,773) contains no alumina domains. Only a very small amount of alumina domains is found after calcination at 1073 K. In line with the larger tendency of tetrahedral Al in ASA(5/95) to agglomerate, the amount of alumina domains is higher for ASA(5/95,773) and ASA(5/95,1073). In general, the higher the aluminium content of the ASA, the higher the amount of alumina domains. The contribution of alumina domains is higher for the full synthesis ASAs than for the ASAs prepared at final pH 3 in an absolute and relative sense. This difference agrees with the finding that surface grafting is dominant until pH 3, whereas precipitation becomes a competing mechanism at higher pH. Furthermore, the amount of alumina domains does not depend strongly on the calcination temperature.

3.3. ASAs prepared by alternative methods

A few other preparation methods to arrive at ASAs were explored. The first one consisted of cogelation of a mixture of sodium silicate in an aqueous aluminium chloride solution. Gelation was brought about by lowering pH to 7. ASA(5/95,cogel) has a surface area of 463 m^2/g and a pore volume of 1.6 ml/g. After exchange of all sodium by ammonium ions, the ^{27}Al NMR spectrum of the dried material (Fig. 14a) shows that aluminium is exclusively present in tetrahedral coordination. In principle, one expects that the aluminium atoms become highly dispersed in the silica particles. When this material is calcined at 923 K, the presence of both five- and six-coordinated Al becomes apparent. Analysis of the ^{27}Al NMR after the adsorption of ammonia shows that the majority of aluminium in this catalyst is part of a mixed silica-alumina phase and only 0.4 wt% Al_2O_3 has segregated to alumina domains. Thus, the aluminium distribution of ASA(5/95,cogel) is quite similar to that of ASA(5/95,3,1073).

The dried precursor to ASA(5/95,fumed) contains already five- and six-coordinated aluminium due to the lower hydroxyl density.

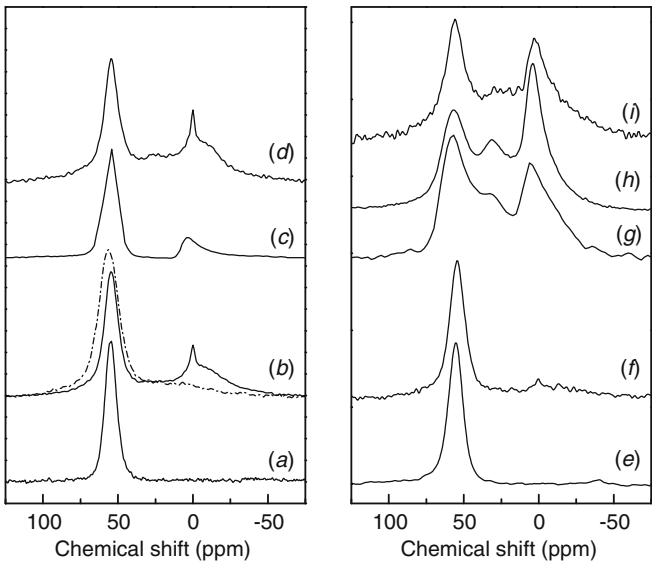

Fig. 14. ^{27}Al NMR spectra of various ASAs: ASA(5/95,cogel,393) (a), ASA(5/95,cogel,923) (b), ASA(20/80,DA,393) (c), ASA(20/80,DA,823) (d), ASA(5/95,F,393) (e), ASA(5/95,F,773), (f), ASA(5/95,fumed,393) (g), ASA(5/95,fumed,773) (h) and ASA(5/95,fumed,1073) (i). For ASA(5/95,cogel), the spectrum after ammonia adsorption is also shown (dashed line).

This difference with ASA(5/95), which contains exclusively four-coordinated Al, implies that the fraction of Al which has been grafted to the already deposited Al or has precipitated should be larger than that in ASA(5/95). Indeed, after calcination at 773 K further agglomeration of aluminium takes place, as follows from the increased contribution of octahedral Al. After calcination at 1073 K, the amount of octahedral Al is lower again. This behaviour is quite similar to that of the HDP ASAs prepared at higher $[Al]_0$. These results suggest that this ASA contains a more substantial amount of alumina domains.

Alumination of a reactive silica surface with ammonium hexafluoroaluminate results in the exclusive formation of tetrahedral Al species. In this synthesis, the pH of an aqueous suspension of silica was adjusted to 9 and grafting was started by the introduction of ammonium hexafluoroaluminate. In the strongly basic solution, octahedral AlF_6^- hydrolyze to tetrahedral $[Al(OH)_4]^-$ species [27] via

$$AlF_6^{3-} + 4OH^- \rightarrow Al(OH)_4^- + 6F^- \quad (9)$$

As the silica surface is negatively charged under these conditions, the dominant deposition mechanism should be direct condensation of $Al(OH)_4^-$ through

$$2{\equiv}SiO^- + [Al(OH)_4]^- + H_2O \rightarrow ({\equiv}SiO)_2 - Al(H_2O)(OH^-) + 3OH^- \quad (10)$$

Upon calcination at 773 K, the coordination of Al does not change as pronouncedly as observed for the other amorphous silica-aluminas. About 90% of aluminium remains tetrahedral and thus a considerable fraction of aluminium resists agglomeration to polymeric forms. The reason for this is not clear. Possibly, strong rearrangements of the silica surface, such as opening of siloxane bonds, can take place under the rather basic conditions and in the presence of fluoride anions. This can give rise to the formation of favourable binding sites for aluminium.

Fig. 14c shows the ^{27}Al NMR spectrum of dried ASA(20/80,DA). The use of the molecular di-*sec*-butoxyaluminotriethoxysilane precursor with preformed Si-O-Al linkages yields an ASA with a higher amount of tetrahedral Al compared to HDP ASAs of similar Al content. The higher fraction of tetrahedral Al (70%) in the dried precursor compared to that of ASA(20/80) (20%) suggests that a large part of the hydrolyzed aluminium-alkoxy groups react with hydrolyzed silicon-alkoxy groups. Nevertheless, due to the faster hydrolysis of aluminium-alkoxy groups compared to silicon-alkoxy groups [17] and the tendency of Al to condense with other Al species, the Al coordination is not purely tetrahedral. Upon calcination at 773 K (Fig. 14d), the fraction of tetrahedral Al strongly decreases to 47%. The distribution in aluminium coordination is then quite comparable to ASA(20/80,3,773).

3.4. Catalytic activity of amorphous silica-aluminas

The acidity of the calcined ASAs was evaluated by determining their catalytic activity in the hydroconversion of *n*-heptane. In the presence of Pd metal, the reaction proceeds by a bifunctional reaction mechanism involving dehydrogenation of the paraffin to an olefin and the reverse hydrogenation as well as the isomerization and cracking of olefins by Brønsted acid sites. There is a general agreement that the isomerization and cracking of alkenes at moderate temperature requires strong Brønsted acid sites [45,46,60,61]. The temperature to obtain an *n*-heptane conversion of 40% (T_{40}) is taken as the activity parameter, because it correlates to the number of Brønsted acid sites when their intrinsic strength is constant [47]. A steam-calcined faujasite zeolite (USY(9.3), T_{40} = 506 K) and a commercial ASA calcined at 773 K (T_{40} = 623 K) and 1073 K (T_{40} = 613 K) were used as reference catalysts.

The kinetic parameters of *n*-heptane hydroconversion for the set of ASAs are presented in Table 7. The HDP ASAs exhibit comparable acid activity to industrial ASAs. The acid activity of ASAs is considerably lower than that of a USY zeolite. Assuming constant acidity of the acid sites, this result implies that the acid site density of ASAs is at least two orders of magnitude lower. The Brønsted acidity of the various ASAs is very similar. ASAs calcined at 1073 K are more acidic than those calcined at 773 K. The differences as a function of the aluminium concentration are relatively small. The one notable exception in this series is the low activity of ASA(1/99,1073) which was about four times less active than ASA(5/95,1073). In general, the acidities of ASAs prepared at final pH 3 are slightly more acidic than their companions synthesized following the completion of urea decomposition, albeit that the most acidic catalyst is ASA(15/85,1073). The activity of ASA(5/95,fumed) is very similar to that of ASA(5/95,773). ASA(5/95,F) has a very low acidity. The two most acidic ASAs are ASA(5/95,cogel) and ASA(20/80,DA).

3.5. Surface structure and Brønsted acidity of amorphous silica-aluminas

A common preparation method for ASAs consists of the grafting of Al to a silica surface. Here, the controlled grafting of aluminium to a reactive silica aerogel with a hydroxyl density of about 4 OH/nm^2 was investigated following the homogeneous release of hydroxyl anions through urea decomposition starting from pH ~2. Two sets of ASA precursors with increasing aluminium content were prepared in this manner. In the preparation of the first set, the deposition of aluminium was carried out until all urea was decomposed. The deposition of aluminium was stopped when the pH reached a value of 3 in the preparation of the second set. The surface of the dried precursors is occupied by a variety of Al species depending on the final pH and $[Al]_0$. At pH 3 and relatively low Al content, the surface contains mainly monopodal Al^{VI} and bipodal Al^{IV} (structures *2* and *4* in Fig. 4). An increase of pH to about 6 results in the exclusive presence of four-coordinated Al. The change in coordination is due to further condensation of the grafted Al with the surface silanol groups, although some grafting of an Al_{13} complex is suspected. When, at pH 3, $[Al]_0$ is increased, the surface will also contain Al^{VI} that has been grafted to bipodal Al^{IV} (structure *6*) and monopodal Al^{VI} (*e.g.* due to the reaction of $Al(H_2O)_5(OH^-)^{2+}$ with structure *2*). The aluminium loading is limited to approximately 12 wt% Al_2O_3 in this case. This loading corresponds to a molar silanol/Al ratio of approximately 1. When the pH is further increased, the rest of Al is deposited below pH 5. Therefore, it is reasonable to expect that the majority of Al species are grafted to the already present surface Al species. At higher loading, some precipitation of aluminium hydroxides occurs as follows from the less homogeneous Al distribution by electron microscopy analysis. The Al species tend to form an increasingly polymeric aluminium hydroxide network with increasing $[Al]_0$.

Table 7
Catalytic activities of *n*-heptane hydroconversion of Pd-loaded support materials (N'_{iso} is proportional to the number of Brønsted acid sites and defined as unity for ASA(5/95,773)).

Catalyst	773 K			1073 K		
	T_{40} (K)	E_{act} (kJ/mol)	N'_{iso}	T_{40} (K)	E_{act} (kJ/mol)	N'_{iso}
ASA(5/95)	630	132	1.0	618	130	1.6
ASA(10/90)	630	125	1.4	618	127	1.9
ASA(15/85)	625	129	1.4	604	128	3.5
ASA(20/80)	626	136	1.0	611	128	2.5
ASA(5/95,3)	620	129	1.3	612	133	2.0
ASA(10/90,3)	622	130	1.5	612	131	2.2
ASA(15/85,3)	627	131	1.2	612	126	2.6
ASA(20/80,3)	625	134	1.1	608	125	3.2
ASA(5/95,fumed)	628	132	1.1	626	127	1.4
ASA(5/95,cogel)[a]	599	120	5.5			
ASA(5/95,F)	652	132	0.4			
ASA(20/80,DA)[b]	598	131	4.0			
ASA(1/99)				659	130	0.37
ASA(comm)	623	129	1.5	613	128	2.3
USY(9.3)	506	128	473			

[a] Calcined at 923 K.
[b] Calcined at 823 K.

Calcination results in a redistribution of the surface aluminium species. Firstly, the diffusion of aluminium into the silica network generates the necessary $Si^{4+} \rightarrow Al^{3+}$ substitutions to induce Brønsted acidity [3,4,7,28] as follows from the acid activity measurements. Alternative models to explain acidity do not seem to be consistent with our results. A correlation of the acidity neither with the amount of the grafted Al [5–10] nor with five-coordinated aluminium [11,12] is evident. Crépeau et al. [10] suggest that such Brønsted acid sites in ASAs have an intrinsic acidity close to that of zeolites. Combined with the present catalytic activity results, this implies that the much lower activity of ASAs is due to their very low acid site density. Thus, only a very small fraction of tetrahedral Al as detected by ^{27}Al NMR spectroscopy gives rise to Brønsted acid sites [31]. It implies that the extent of diffusion of Al into silica is very limited. Due to the very low concentration of such BAS, spectroscopic identification of these sites has not been achieved yet [10]. The small variation in the acidity in the present suite of ASAs makes it difficult to draw pertinent conclusions about the genesis of Brønsted acid sites. Nevertheless, the increase in the surface acidity with calcination temperature is reasonably explained by the diffusion of more Al into the silica network. This effect of the calcination temperature was earlier discussed by Boehm and Schneider [28]. The acidity does not vary much with aluminium concentration for the ASAs as long as the surface of the precursor is fully covered with aluminium species. In accordance with this, only an appreciably lower Al content results in a much lower acidity. The ASAs prepared at final pH 3 are more acidic than their complete synthesis counterparts. This difference is particularly evident for ASA(5/95) and ASA(10/90) after calcination at 773 K. It suggests that monopodal octahedral Al is a better precursor to the formation of Brønsted acid sites than bipodal tetrahedral Al. A reason is perhaps that bipodal Al^{IV} represents a stable surface arrangement less conducive to the rearrangements of the silica surface required to facilitate the diffusion of Al into the silica than the more loosely grafted Al^{VI}. Indeed, the acidity of ASA(5/95,F), which contains quite stable tetrahedral Al sites as follows from the minor changes in the ^{27}Al NMR spectrum upon calcination, is very low. Finally, the higher acidity of ASA(5/95,cogel) may be due to the higher amount of Al ending up in the silica network because the silica network is formed during the deposition of Al. This also explains the higher acidity of ASA(20/80,DA).

Secondly, the surface Al species tend to agglomerate and partially form small patches of aggregated aluminium oxide. The dried precursors prepared after the completion of urea decomposition contain about 5 wt% tetrahedral Al. Calcination results in the agglomeration of Al. Part of the octahedral Al atoms do not change their coordination upon ammonia adsorption, because they are part of a separate alumina phase. Typically, the contribution of such a phase is calculated on the basis of an assumed fixed Al^{IV}:Al^{VI} ratio of 3:7 in transition aluminas. From the R^2 NMR measurements, it follows that such alumina domains only contain octahedral Al. This octahedral Al phase can be probed quantitatively by their inaccessibility to ammonia. Only for an ASA with a substantially higher Al content, *i.e.* ASA(55/45), a free transition alumina

phase is readily apparent from R^2 NMR measurements. All tetrahedral Al is part of the mixed silica-alumina phase for the HDP ASAs.

The amount of such segregated domains of aluminium oxide increases with the aluminium concentration. The formation of alumina domains is only completely avoided in ASA(5/95,3,773) for which the deposition of Al is fully dominated by the grafting of Al to silanol groups. Even so, a small fraction of Al segregates into an aluminium oxide phase upon calcination at 773 K. The surface of ASA(5/95,3,773) can be considered a pure amorphous silica-alumina phase. It contains monopodal octahedral Al and bipodal tetrahedral Al. Octahedral Al atoms become tetrahedrally coordinated upon ammonia adsorption. ASA(5/95) contains a slightly higher amount of aluminium. All Al is tetrahedrally coordinated in this sample. Calcination of this precursor at 773 K induces the segregation of about 30% of Al into aluminium oxide domains. This segregation could be due to the higher Al density on the surface, but also to the suspected presence of a small amount of Al_{13} complexes with the Keggin structure, which may have been deposited above pH 3. In any case, calcination of ASA(5/95) at 473 K already results in octahedral Al, indicating surface mobility and agglomeration. With increasing Al concentration, the amount of segregated Al increases. This trend is more pronounced for the complete synthesis ASAs, which contain more aluminium, than for their counterparts prepared until pH 3. The formation of a considerable amount of the segregated aluminium oxide domains in ASA(15/85) and ASA(20/80) agrees with the structural model of a polymeric aluminium hydroxide phase being grafted above pH 3 upon the first layer of the grafted aluminium. The R^2 NMR measurements suggest that this phase does not convert to a transition alumina phase, but consists of a polymeric network of octahedral Al.

After calcination, the ASAs contain varying amounts of five-coordinated aluminium. Fig. 15 evidences a strong correlation between the amount of Al^V probed by ^{27}Al NMR and the content of alumina domains. This correlation confirms the assumption that five-coordinated Al forms the interface between the domains of the segregated octahedral Al atoms and the mixed silica-alumina phase as proposed earlier [31]. It is finally worthwhile to mention that the amount of Al^V is comparable to the amount of Al in the alumina domains, which implies that the size of the domains should be small.

The surface model for a typical amorphous silica-alumina which arises from this study contains two major ingredients, *i.e.* (i) a mixed silica-alumina phase and (ii) domains of segregated octahedral Al. The aluminium speciation in the mixed amorphous silica-alumina phase is as follows:

- Four-coordinated Al species. These share two oxygen atoms with the silica network (structure *4* in Fig. 4). In accord with this, the amount of Al^{IV} never exceeds the amount corresponding to a molar silanol/Al ratio of 2 in the calcined materials prepared by homogeneous deposition–precipitation.
- Six-coordinated Al species. Some are isolated and coordinate to one oxygen anion of the subjacent silica support (structure *2* in Fig. 4), others have agglomerated to some extent forming one or perhaps more Al–O–Al linkages (*e.g.* the octahedral Al in structure *10* in Fig. 4). Upon ammonia adsorption, this form of octahedrally coordinated Al becomes tetrahedrally coordinated. A small fraction of octahedrally coordinated Al is present at the interface between the mixed phase and the alumina domains. These octahedral Al species become five-coordinated upon ammonia adsorption.
- Five-coordinated Al species. These are at the interface between the mixed silica-alumina phase and the domains of aluminium oxide.

The aluminium oxide phase is present as very small domains containing only octahedral Al. This form of Al is not accessible by NH_3 which allows their quantification by ^{27}Al NMR. The aluminium oxide phase is connected to the mixed silica-alumina phase by five-coordinated aluminium. This surface model seems to be applicable for the wider range of ASAs synthesized in this study.

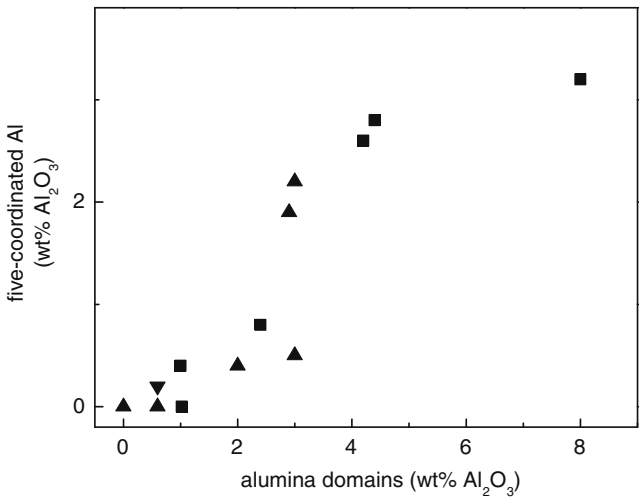

Fig. 15. Relation between the amount of five-coordinated aluminium as observed by ^{27}Al NMR spectroscopy after ammonia adsorption and the amount of segregated aluminium oxide domains: ASAs prepared following completion urea decomposition (■), ASAs prepared at a final pH of 3 (▲) and ASA(5/95,cogel) (▼).

4. Conclusion

It is possible to prepare amorphous silica-aluminas via homogeneous deposition–precipitation of aluminium on a silica surface followed by calcination. These ASAs exhibit similar Brønsted acidity as industrial amorphous silica-aluminas prepared by the grafting of aluminium on very reactive silica gels. Their acidity does not vary systematically with the aluminium concentration, except at aluminium contents below 5 wt% Al_2O_3. The acidity increases with increasing calcination temperature. The active sites form due to the diffusion of aluminium into the silica network at high temperatures, leading to Al substitutions for Si atoms. This is expected, as the acidity does not correlate with anything else, *viz.*, the amount of four-coordinated aluminium nor the presence of segregated Al or five-coordinated aluminium at the interface of these domains and the silica-alumina phase. Deposition occurs predominantly via hydrolytic adsorption of aluminium to the hydroxyl groups on the silica surface and already grafted aluminium. Precipitation becomes more significant at higher aluminium concentration. After grafting, the surface contains four- and six-coordinated aluminium as well as domains of a more polymeric form of aluminium hydroxides. Calcination results in two competing processes, namely the diffusion of aluminium into the silica network and sintering of aluminium into separate domains of a phase in which octahedral Al is dominant. The surface of an amorphous silica-alumina consists of isolated aluminium grafted to the silica surface (pure silica-alumina phase), domains of aluminium oxides and a very small amount of aluminium in the silica network, which brings about the Brønsted acidity.

Acknowledgments

The authors gratefully acknowledge the financial support from Shell Global Solutions. The authors are very thankful to Dr. Ralph Haswell of Shell Global Solutions for TEM and SEM measurements.

Appendix A. Supplementary data

Supplementary data associated with this article can be found, in the online version, at doi:10.1016/j.jcat.2009.11.008.

References

[1] J. Ward, Fuel Process. Technol. 35 (1993) 55.
[2] J. Scherzer, A.J. Gruia, Hydrocracking Science and Technology, Dekker, New York, 1996. p. 215.
[3] C.L. Thomas, Ind. Eng. Chem. 41 (1949) 2564.
[4] M.W. Tamele, Disc. Faraday Soc. 8 (1950) 270.
[5] J.H. De Boer, Disc. Faraday Soc. 52 (1971) 109.
[6] K.G. Miesserov, J. Catal. 13 (1969) 169.
[7] R.S. Hansford, Ind. Eng. Chem. 39 (1947) 849.
[8] M. Trombetta, G. Busca, S. Rossini, V. Piccoli, U. Cornaro, A. Guercio, R. Catani, R.J. Willey, J. Catal. 179 (1998) 581.
[9] W. Daniell, U. Schubert, R. Glockler, A. Meyer, K. Noweck, H. Knözinger, Appl. Catal. A 196 (2000) 247.
[10] G. Crépeau, V. Montouillout, A. Vimont, L. Mariey, T. Cseri, F. Maugé, J. Phys. Chem. B 110 (2006) 15172.
[11] C.-P. Hwang, C.-T. Yeh, J. Catal. 182 (1999) 48.
[12] S. Blonski, S.H. Garolfini, J. Phys. Chem. 100 (1996) 2201.
[13] J.A. Rabo, G.J. Gajda, Catal. Rev.-Sci. Eng. 31 (1989) 385.
[14] R. Brace, E. Matijevic, Colloid Polym. Sci. 255 (1977) 153.
[15] United States Patent 3536605, 1968.
[16] R. Mokaya, W. Jones, J. Mater. Chem. 9 (1999) 555.
[17] C.J. Brinker, G.W. Scherer, Sol–Gel Science. The Physics and Chemistry of Sol–Gel Processing, Academic Press, San Diego, 1990.
[18] J.W. Kriesel, M.S. Sander, T.D. Tilley, Chem. Mater. 13 (2001) 3554.
[19] J.W. Kriesel, M.S. Sander, T.D. Tilley, Adv. Mater. 13 (2001) 331.
[20] P. Cloos, A.J. Leonard, J.P. Moreau, A. Herbillon, J.J. Fripiat, Clays Clay Miner. 17 (1969) 279.
[21] A. Leonard, S. Suzuki, J.J. Fripiat, C. de Kimpe, J. Phys. Chem. 68 (1964) 2608.
[22] J.J. Fripiat, A. Leonard, J.B. Uytterhoeven, J. Phys. Chem. 69 (1965) 3274.
[23] R.K. Iler, The Chemistry of Silica, Wiley-VCH, Weinheim, 1979.
[24] J.W. Geus, A.J. van Dillen, in: G. Ertl, H. Knözinger, J. Weitkamp (Eds.), Preparation of Solid Catalysts, Wiley-VCH, Weinheim, 1999 (Chapter 4.6).
[25] R.J.M.J. Vogels, J.T. Kloprogge, J.W. Geus, J. Colloid Interface Sci. 285 (2005) 86.
[26] A. Samoson, E. Lippmaa, G. Engelhardt, U. Lohse, H.-G. Jerschkewitz, Chem. Phys. Lett. 134 (1987) 589.
[27] H.-M. Kao, C.-C. Ting, S.-W. Chao, J. Mol. Catal. A 235 (2005) 200.
[28] H.P. Boehm, M. Schneider, Z. Anorg. Chem. 316 (1962) 128.
[29] K.J.D. MacKenzie, J. Temuujin, K. Okada, Thermochim. Acta 327 (1999) 103.
[30] K.J.D. MacKenzie, J. Temuujin, M.E. Smith, P. Angerer, Y. Kameshima, Thermochim. Acta 359 (2000) 87.
[31] M.F. Williams, B. Fonfé, C. Sievers, A. Abraham, J.A. van Bokhoven, A. Jentys, J.A.R. van Veen, J.A. Lercher, J. Catal. 251 (2007) 485.
[32] W.E.E. Stone, G.M.S. El Shafei, J. Sanz, S.A. Selim, J. Phys. Chem. 97 (1993) 10127.
[33] B.M. de Witte, P.J. Grobet, J.B. Uytterhoeven, J. Phys. Chem. 99 (1995) 6961.
[34] M.P.J. Peeters, A.P.M. Kentgens, Solid State Nucl. Magn. Reson. 9 (1997) 203.
[35] J.-P. Gilson, G.C. Edwards, A.W. Peters, K. Rajagopalan, R.F. Wormsbecherp, T.G. Roberie, M.P. Shatlock, J. Chem. Soc. Chem. Commun. (1987) 91.
[36] J. Sanz, A. Madani, J.M. Serratosa, J.S. Moya, S. Aza, J. Am. Ceram. Soc. 71 (1988) 418.
[37] A. Omegna, J.A. van Bokhoven, R. Prins, J. Phys. Chem. B 107 (2003) 8854.
[38] D. Coster, J.J. Fripiat, J. Chem. Mater. 5 (1993) 1204.
[39] T.E. Wood, A.R. Siedle, J.R. Hill, R.P. Skajune, C.J. Goodbrake, J. Mater. Res. Soc. Symp. Proc. 180 (1990) 97.
[40] S.M. Bradley, R.A. Kydd, R.F. Howe, J. Colloid Interface Sci. 159 (1993) 405.
[41] S. Acosta, R.J.P. Corriu, D. Leclercq, P. Lefevre, P.H. Mutin, A. Vioux, J. Non-Cryst. Solids 170 (1994) 234.
[42] Y. Mizushima, M. Hori, J. Non-Cryst. Solids 167 (1994) 1.
[43] E. Bourgeat-Lami, P. Massiani, F.D. Renzo, P. Espiau, F. Fajula, Appl. Catal. A 72 (1991) 139.
[44] J.A. van Bokhoven, A.M.J. van der Eerden, D.C. Koningsberger, Stud. Surf. Sci. Catal. 142 (2002) 1885.
[45] G.E. Gianetto, G.R. Perot, M.R. Guisnet, Ind. Eng. Chem. Prod. Res. Dev. 25 (1986) 481.
[46] J.W. Thybaut, C.S. Laxmi Narasimhan, J.F. Denayer, G.V. Baron, P.A. Jacobs, J.A. Martens, G.B. Marin, Ind. Eng. Chem. Res. 44 (2005) 5159.
[47] E.J.M. Hensen, D.G. Poduval, D.A J.M. Ligthart, J.A.R. van Veen, M.S. Rigutto, submitted for publication.
[48] R.J.M.J. Vogels, G. Caminiti, V. Crisponi, A. Nurchi, Z. Lai, Z. Naturforsch. A 39 (1984) 1235.
[49] J.W. Akitt, A. Farthing, J. Chem. Soc. Dalton Trans. (1981) 1624.
[50] J.W. Akitt, J.M. Elders, X.L.R. Fontaine, A.K. Kundu, J. Chem. Soc. Dalton Trans. (1989) 1889.
[51] J.T. Kloprogge, D. Seykens, J.B.H. Jansen, J.W. Geus, J. Non-Cryst. Solids 152 (1993) 207.
[52] C.F. Baes, R.E. Mesmer, The Hydrolysis of Cations, John Wiley, New York, 1976. p. 112.
[53] A.V. Plyasunov, I. Grenthe, Geochim. Cosmochim. Acta 58 (1994) 3561.
[54] J.W. Akitt, Prog. Nucl. Magn. Reson. Spectrosc. 21 (1989) 1.
[55] G. Fu, L.F. Nazar, A.D. Bain, Chem. Mater. 3 (1991) 602.
[56] J.D. Danforth, J. Phys. Chem. 59 (1955) 564.
[57] R.H. Meinfold, R.C.T. Slade, R.H. Newman, Appl. Magn. Reson. 4 (1993) 121.
[58] D.P. Raleigh, M.H. Levitt, R.G. Griffin, Chem. Phys. Lett. 146 (1988) 71.
[59] A. Abragam, The Principles of Nuclear Magnetism, Oxford University Press, Oxford, 1961.
[60] A. Van de Runstraat, J.A. Kamp, P.J. Stobbelaar, J. van Grondelle, S. Krijnen, R.A. van Santen, J. Catal. 171 (1997) 77.
[61] V.M. Akhmedov, S.H. Al-Khowaiter, Catal. Rev. Sci. Eng. 1 (2007) 33.